Contract No:

This document was prepared in conjunction with work accomplished under Contract No. DE-AC09-08SR22470 with the U.S. Department of Energy.

Disclaimer:

SRNL LDRD Annual Report 2008

SRNL™
SAVANNAH RIVER NATIONAL LABORATORY
Operated by Savannah River Nuclear Solutions, LLC
We Put Science To Work

Table of Contents

Letter from the Director…… 2

Project Summaries Full Projects …… 3
Advanced Li-Glass Scintillation Materials for Neutron Detection ……..... 4
A System-Level Evaluation of Interactions between Environmental Factors and Cyanobacterial Hydrogen Production ……..…….. 5
Chemical Reactivity and Phase Behavior of the Pu-Zr System …….. 7
Development of Hydrogen Compatible Ultra-Pure High-Strength Alloy Steels……. 9
Effect of Pretreatment on Pt-Co Cathode Catalysts for the Oxygen-Reduction Reaction…….. 11
High Performance Catalyst Support Materials for Fuel Cells …… 14
Ionic Liquid Electrochemical Separations …….....16
Life Span of Novel Biopolymer Sequestering Agents for Organic and Inorganic Contaminants ……. 17
Novel Electrochemical Process for High Capacity Energy Storage …….. 19
Novel Nanostructured Anode Materials for Li-Ion Rechargeable Batteries with High Capacity and Inherent Safety ……... 21
Rate of Eutectic Formation in Plutonium-Stainless Steel Couples …… 22
Real-Time Airborne Beryllium Particulate Monitor …….. 23
Separation of the Transuranic Actinides from the Lanthanides Using HDEHP …… 25
Stable Isotope Nitrogen-15 Production …….. 27
Structural Interactions of Hydrogen with Bulk Amorphous Microstructures …… 29
Systems Microbiology for Energy and the Environment: Structural and Functional Analysis of *Kineococcus radiotolerans* Genome …….. 30
Understanding Compositional and Kinetic Drivers for Nepheline Crystallization in High-Level Waste Glasses …….....32
Zero Interface Catalyst Impregnated Ionomer Membranes for Fuel Cell Applications ……33

Project Summaries Quick Hits ……....34
Acceleration of Ion Exchange Kinetics …….. 35
Enhanced Stabilization and Packaging of Challenging Materials …… 37
Improving Operational Forecasts by Incorporation of Non-Standard Weather Data …… 39
Structural and Electrical Characterization of Organic Materials in Organic-Based Devices…. 41
The Effect of Magnetic Field and Magnetic Field Type on the Uranium and Strontium Sorption on Monosodium Titanate …….....44

We Put Science To Work™

From the Laboratory Director

I am pleased to have the opportunity to present the 2008 Laboratory Directed Research and Development (LDRD) annual report. This is my first opportunity to do so, and only the second such report that has been issued. As will be obvious, SRNL has built upon the excellent start that was made with the LDRD program last year, and researchers have broken new ground in some important areas.

In reviewing the output of this program this year, it is clear that the researchers implemented their ideas with creativity, skill and enthusiasm. It is gratifying to see this level of participation, because the LDRD program remains a key part of meeting SRNL's and DOE's strategic goals, and helps lay a solid scientific foundation for SRNL as the premier applied science laboratory.

I also believe that the LDRD program's results this year have demonstrated SRNL's value as the EM Corporate Laboratory, having advanced knowledge in a spectrum of areas, including reduction of the technical risks of cleanup, separations science, packaging and transportation of nuclear materials, and many others. The research in support of Energy Security and National and Homeland Security has been no less notable.

SRNL's researchers have shown again that the nascent LDRD program is a sound investment for DOE that will pay off handsomely for the nation as time goes on.

Dr. Samit K. Bhattacharyya
Laboratory Director

SRNL
SAVANNAH RIVER NATIONAL LABORATORY
TM

Project Summaries Full Projects

Advanced Li-Glass Scintillation Materials for Neutron Detection

R. A. Sigg, D. M. Missimer and A. R. Jurgensen

Federal agencies are seeking enhanced solid state neutron detectors that will improve performance in hand-held radiation detection instruments such as those used by first-responder personnel. The agencies need detectors that are more efficient, less expensive and more rugged than small ^{3}He detectors, and that reject gamma-ray interferences better than current commercially-available neutron-sensitive scintillators. Since the detection of neutrons indicates the possible presence of threat materials, it is important avoid false positives.

SRNL is studying Li-glass scintillators that reject gamma-ray interferences better than other solid-state devices. The energy resolution of ~7.5% FWHM for the ^{6}Li(n,)T interaction peak is much better than the 14% or greater claimed for other neutron-sensitive scintillation materials. When advantage is taken of the resolution by using the material as a spectrometer rather than as a gross counter, gamma-ray interferences are significantly reduced.

In preparing the glass materials, SRNL is studying the effects of

- Melting and heat treatment protocols
- Oxidation state control for the primary scintillant
- Elemental composition of seven glass scintillator materials

to assure that the enhanced performance can be duplicated and potentially improved.

Within experimental uncertainties, photon emission from three of the seven glasses equal and possibly exceed that observed from material provided by NucSafe, LLC.

First year LDRD seed funding contributed to securing funding from NA22 and second-year LDRD. Plans for FY09 include

- Preparation of additional glasses using enriched 6Li
- Neutron resolution and efficiency measurements using known fluxes at the HP Calibration Laboratory
- Improved oxidation-state control
- Application of x-ray photoelectron spectroscopy to determining Ce^{+4} : Ce^{+3} ratios
- Measuring fluorescence lifetimes, and excitation and emissions spectra
- Electron microscopy studies.

A System-Level Evaluation Of Interactions Between Environmental Factors And Cyanobacterial Hydrogen Production

Chris M. Yeager, Christopher Bagwell, Charlie Milliken, Sarah Harcum, Lauren Staples, Tommy Sessions

The goal of this continuation LDRD project is to develop and utilize system-level molecular biological techniques to investigate the interactions between H_2 producing cyanobacteria and their commonly associated bacterial flora.

Hydrogen energy development is one of DOE's top priorities, and developing an economically and environmentally sound H_2 production process is an important part of the Department's vision. Biological H_2 production by cyanobacteria or green algae is a highly attractive option in that it represents a renewable resource requiring only water, sunlight, air, and trace mineral salts. This process does not use or produce hazardous materials, is considered a carbon-neutral or –negative process, and could be coupled to the production of other commodities.

Most research efforts aimed at understanding and producing biohydrogen directly from sunlight have focused on developing operational, hydrogen producing bioreactors or conducting detailed molecular analysis of genes and proteins from several model organisms that were isolated decades ago. However, based on an extensive literature search and the recommendations of several recent DOE- and DOD-sponsored expert review panels it is obvious that an important element of the research continuum from genes to H_2-producing bioreactors has been largely overlooked - the physiology and diversity of naturally occurring, H_2-producing phototrophs**.** It is astonishing that our knowledge of photobiological H_2 production comes from just a handful of strains, when it is obvious that many thousands, or even millions, of species possessing this ability exist in nature. From a biotechnological perspective, it makes sense to explore (and potentially harness) the untapped diversity of H_2-producing capabilities that have been naturally evolving for billions of years.

Cyanobacteria are almost always closely associated with other bacteria. Indeed, many strains of cyanobacteria cannot be isolated and grown in the absence of bacterial associates, and for those cyanobacterial strains that can be isolated, it is extremely difficult to maintain them as pure cultures. The relationship between cyanobacteria and their bacterial associates can be mutually-beneficial, antagonistic, or specific to select cellular processes (e.g. H_2 production), but in all cases very little detail is known about these interactions. Increased knowledge of cyanobacterial interactions with their commonly associated bacteria will advance the utility of these microorganisms for energy production. The goals of this LDRD project are to 1) assess the gross physiological effects (growth rate, growth yield, H_2 production, photochemical efficiency, etc.) imparted by bacterial associates and environmental factors on cultures of H_2 producing cyanobacteria in a bioreactor and 2) characterize the effect of glucose and light on H_2 producing cyanobacteria through physiological and gene expression analysis.

A systematic method of preparing cyanobacterial cells for H_2 evolution assays was established. Cyanobacteria were cultured in Roux flasks (2L) containing $BG11^-$ media bubbled rapidly with air under a light/dark photocycle (16:8). To assay biological hydrogen production we are using an effective H_2 analysis platform consisting of: a dual GC system to simultaneously measure H_2, O_2, N_2, CO_2, and C_2H_4 (ppm), an O_2/H_2 electrode to provide instantaneous rates of H_2 or O_2 evolution/uptake. Using this platform we screened ~75 bacteria isolated from cyanobacterial enrichment cultures or BSC cyanobacterial filaments for their ability to enhance or inhibit cyanobacteial growth. Five strains significantly inhibited growth of *Anabaena* PCC 7120, several impart a slight growth advantage. Initial experiments suggest that several of the strains that inhibit growth of *Anabaena PCC 7120* are biocidal towards this and other cyanobacteria. Further research is necessary to identify the mechanism of action and to evaluate the potential commercial application of these strains as algicides.

The effect of light and exogenous glucose on H_2 production was examined among 10-12 diverse cyanobacterial strains. Glucose stimulated H_2 production rates and yield in the majority of strains; 2-12 fold increase in rates and 2-40 fold increase in yields. CO_2 stimulated rates of H_2 production up to 3 fold and yields to 8 fold, but inhibited H_2 production in some strains. In many strains, glucose-dependent H_2 production rates and yield were not greatly stimulated by increases in light intensity >100 µmol m^{-2} h^{-1}. Batch cultures of *Anabaena* PCC 7120 were grown phototrophically with (mixotrophic) or without (autotrophic) glucose. Measurements of cell density, pH, glucose concentrations, organic

metabolites, and heterocyst frequency were taken. During mixotrophic conditions, glucose consumption appeared to be limited. Addition of low amounts of organic carbon may effectively support H_2 production. Addition of organic carbon can greatly increase H_2 production in select cyanobacteria. The commonly held belief that the economic feasibility of cyanobacterial H_2 production is dependent primarily on the light to H_2 conversion efficiency is fundamentally flawed. Mixotrophic growth or incubations should be explored as a means to produce bioenergy and/or bioproducts using bacterial phototrophs.

Chemical Reactivity and Phase Behavior of the Pu-Zr System

G. F. Kessinger, A. R. Jurgensen, P. M. Almond

Objective: The objective of this project is to synthesize actinide-zirconium alloys and investigate their chemical reactivity in nitric acid solutions.

The significance of these alloy materials (which have been utilized as reactor fuels) to on-going work in the DOE complex is two-fold. First, as part of the on-going nuclear material stabilization activities in H-Area (at SRS), numerous zirconium-plutonium fuels are being treated. The present protocol for stabilization of these fuels call for burning the materials in air, to produce PuO_2 and ZrO_2, followed by dissolution of the oxides. Second, technology development associated with GNEP spent nuclear fuel aqueous reprocessing flowsheets is predominately based on head-end dissolution of spent fuels in nitric acid. Since the fuels projected to be reprocessed include actinide-Zr fuels containing predominately U and Pu, with lesser amounts of Np, Am, and Cm, the reactivity of these alloy fuels in nitric acid is of paramount importance.

The reactivity of U-Zr alloys with nitric acid was first investigated during the 1950s. During those investigations, it was shown that U-Zr alloys containing 2 to 40 atomic percent Zr, which have not been quenched at 725°C or higher, have the ability to react explosively when treated with nitric, hydrochloric, or citric acids. It was concluded that the explosively-reacting materials were two-phase mixtures of α-U and UZr_3, from which the α-U had been leached by the nitric acid, leaving the UZr_3 in a high surface area, shock-sensitive configuration. The resulting trizirconide reacts fast (explosively) when the reaction is initiated by a spark or even jostling the material. As this reactivity was studied more extensively, investigations showed that the addition of adequate fluoride ion to the nitric acid (6:1 ratio F^-:Zr, utilizing HF or a soluble alkali metal fluoride salt) facilitated dissolution of the trizirconide phase at a rate comparable to that of the α-U. It has long been assumed that the kappa plutonium-zirconium phase ($PuZr_3$) and the ternary ($U_xPu_{1-x}Zr_3$) phase also behave in an analogous fashion, and there is anecdotal evidence of energetic reactions of these phases with nitric acid. Unfortunately, little is understood about the phase behavior and chemical reactivity of mixed actinide zirconium ternary and higher systems, such as U-Pu-Zr or U-Pu-An-Zr (An = Np, Am, and/or Cm).

The binary U-Zr phase diagram is well characterized, and the systems Pu-Zr[1,2,3,4] and Np-Zr [5,6,7] have been studied to a lesser extent than U-Zr, but the Am-Zr, and Cm-Zr systems are poorly characterized. Recent evaluations of the Pu-Zr system (during the 1990's) call into question the existence of the binary $PuZr_3$ phase (which is a phase of great importance if these fuels are to be processed with dissolution flowsheets based on nitric acid). During the 1990's, study of the Np-Zr system indicated that Np and Zr may be immiscible over a broad compositional range. There also appear to be miscibility issues related to the Am-Np system[8] as well; however, it is not known if this immiscibility would impact the miscibility of these metals in the more complex U-Pu-Np-Am-Cm-Zr solid solution. Knowledge of the phase behavior of the Am-Zr and Cm-Zr systems is even less developed than that for Np-Zr, so it is not known if similar miscibility issues are present in these two binary phases. Miscibility gaps could indicate that minor actinide-containing alloy fuels might not be suitable for reactor use due to solid solution phase instability, so it is imperative that the phase behavior of the prospective fuel alloys be characterized.

During the past year, efforts were directed toward the development of the experimental techniques necessary to synthesize alloys. These activities included:

- development of an experimental plan to safely handle finely-divided metal and metal hydrides, both of which are reactive with ambient air
- procurement, testing, and set-up of experimental equipment (tube furnace and pellet press);
- upgrading of a facility glovebox to accommodate experimental equipment;
- pressing mixed hydride pellets;
- calcining pellets under inert atmosphere;
- characterization of pellets by X-ray diffraction.

The tube furnace was bench tested before installation in the radioactive glovebox. Prior to furnace installation, the radioactive glovebox was upgraded to increase the exhaust flow through the box. After successful completion of the ventilation upgrade, the furnace was installed, again tested, and found to be operational. After cold testing, the hydraulic pellet press was installed in an inert gas glovebox and pellets were pressed. The pressed pellets were successfully transferred and calcined.

Conclusion The methodology for synthesis and characterization of actinide-zirconium alloys has been successfully developed for synthesis of actinide-zirconium alloys via a pathway involving the decomposition of hydrides. Pellet pressing, sample transfer, and calcination steps have been successfully demonstrated using uranium as a surrogate for the higher actinides. The logical continuation of this project is the demonstration of the technique with the higher actinides.

Literature Cited

[1] Y. Suzuki, A. Meada and T. Ohmichi, *J. Alloys Compounds*, 182, L9 (1992).
[2] H. Okamoto, *J. Phase Equilibria, 14*, 400 (1993).
[3] A. Maeda, Y. Suzuki, Y. Okamoto and T. Ohmichi, *J. Alloys Compounds*, 205, 35 (1994).
[4] H. Okamoto, *J. Phase Equilibria, 16*, 287 (1993).
[5] J.K. Gibson and R. G. Haire, *J. Nucl. Mater., 201*, 225 (1993).
[6] J.K. Gibson et al., *J. Alloys Compounds*, 213/214, 106 (1994).
[7] J.K. Gibson, R. G. Haire and T. Ogawa, *J. Nucl. Mater., 273*, 139 (1999).
[8] J.K. Gibson and R. G. Haire, *J. Nucl. Mater., 195*, 156 (1992).

Development of Hydrogen Compatible Ultra-Pure High-Strength Alloy Steels

M. J. Morgan

Objective: The premise of this project was to investigate the compatibility of ultra-pure high-strength HY130 alloy steel for service in high-pressure hydrogen environments. Research at the University of Pennsylvania indicates that the most important metallurgical factors which control the tendency for hydrogen-induced brittle fracture in almost all commercial high-strength alloys are their composition and the degree of impurity segregation to grain boundaries (1). The experiments proposed here will test the hypothesis that hydrogen-induced intergranular fracture in steels can be greatly reduced or eliminated even in high-pressure service by producing ultra-high purity alloys with alloy modifications that minimize impurity segregation.

A high-purity heat of HY130 steel was made at Ames National Laboratory having the composition in weight percent of 0.10 C, 0.47 Cr, <0.01 Mn, 0.50 Mo, 5.12 Ni, 0.004 P, <0.001 S, <0.01 Si, 0.077 V. The heat was modified from commercial grade HY130 steel by reducing the alloy elements Mn and Si to levels as low as possible. Impurity levels (P and S) were also kept to low levels. The steel was heat treated by austenitizing at 850˚C and tempering at 200˚C to a hardness of Rc 36 and yield strength of 1054 MPa.

Researchers at Penn tested it in four-point bending in 20 psi hydrogen gas, which was their maximum achievable pressure. The steel showed remarkable resistance to intergranular fracture and the failure in hydrogen occurred at a K level of 113 ksi√in.

In order to explore higher pressures, C specimens were fabricated and tested in a special chamber at 1500 psi hydrogen at SRNL. The specimen design is shown in Fig. 1 and the results are summarized in Table I. The behavior in hydrogen at this pressure is very sensitive to the loading rate. The maximum K level decreased and the percent intergranular fracture increased when the loading rate was decreased by a factor of ten. In addition, the beneficial effect of a higher tempering temperature, aimed at decreasing the defect concentration at prior austenite grain boundaries, was quite small; however, there was some increase in the maximum K level, corresponding to a small decrease in the amount of intergranular fracture (Fig 2).

To assess whether residual impurities could have played a role in this steel, a specimen was heated in UHV and Auger-analyzed to determine what elements would segregate to the free surface. This would identify the mobile impurities that could possible segregate to grain boundaries. The spectra indicate that sulfur was found upon heating to 350˚C. After ion sputtering to return to a clean surface and heating to 550˚C, a possible presence of phosphorus was found. It may be that these elements played a role in the susceptibility of this steel to HIC.

The conclusion that can be drawn from these results is that this particular heat of steel is probably not pure enough to give a baseline behavior for an ideally pure steel. What is needed for future efforts along this line is a heat of steel made using a melting practice that would eliminate this kind of contamination. At this point, it appears that this is available only at the lab of Professor Abiko in Japan. It is anticipated that such a heat of steel will be obtained in the coming months and that this issue can be re-addressed.

The results show that the 5%NiCrMoV steel with about 0.1% carbon shows promise in regard to safe use in high-pressure hydrogen environments, but especially at around atmospheric pressure. However, we have not yet achieved a purity level high enough to establish the baseline behavior of an ideally pure version of this steel in high-pressure hydrogen. The results of this study were presented and published at the 2008 International Hydrogen Conference (2).

Table I –Thresholds and % Intergranular Fracture (IG)

Temper ºC	Hardness Rc 150 kg	Speed In / min	KTH ksi–$in^{1/2}$	% IG
200	35.5	0.002	69.2	<5%
200	35.5	0.0002	32.4	~35%
400	35.1	0.0002	40.7	~30%

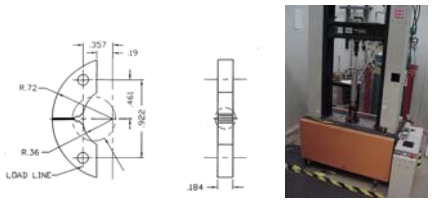

(a) (b)

Figure 1. (a) Design of arc-shaped specimens electric-discharge machined from high-purity HY130 and (b) Pressure vessel mounted on mechanical testing machine SRNL).

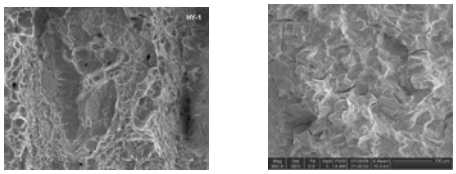

(a) (b)

Figure 2. Fracture Appearance of samples tested in: (a) Dimpled Rupture in Air and (b) Intergranular Fracture in 1500 psi Hydrogen Gas.

1. Y. Takeda and C. J. McMahon, Jr., "Strain Controlled vs. Stress Controlled Hydrogen Induced Fracture in a Quenched and Tempered Steel," Met. Trans. A, 1981, 12A, 1255.

2. C. J. McMahon, Jr., X-Y Liu, J. Kameda, and M. J. Morgan "Recent Observations of Hydrogen-Induced Cracking of High-Strength Steels", 2008 International Hydrogen Conference – Effect of Hydrogen on Materials, Jackson Hole, WY, September 7-10, 2008.

Effect of Pretreatment on Pt-Co Cathode Catalysts for the Oxygen-Reduction Reaction

Elise B. Fox and Hector Colon-Mercado

The use of highly dispersed platinum crystallites on high surface area carbon increases the active surface area and electrocatalytic activity of the electrocatalysts, thereby reducing the Pt loadings in the cell. About four times the loading of the anode is currently used at the cathode to help account for the low activity of the Pt electrocatalyst for the oxygen reduction reaction (ORR). Although improvement in catalytic activity by alloying Pt with transition metals has lead to lower loadings in the cathode, loadings are still one order of magnitude higher than the DOE target for 2015. In order to reduce the precious metal loading without sacrificing activity and stability, a new method for the preparation of bimetallic catalysts is proposed. Currently, Pt-alloy particles, with 2 to 3 nm in diameter, are loaded on high surface area carbon supports. Of the Pt loaded, only the surface atoms interact with the reactants. In order to increase the Pt utilization per metal particle the new process for catalyst preparation will incorporate a non-noble transition metal core coated with a skin layer of Pt deposited on high surface area carbon. This approach was proved by Mukmirovic et al [1], demonstrating an enhancement of catalytic activity and stability of Pt/Pt alloys monolayers by galvanic displacement of a copper monolayer on a palladium single crystal and on palladium particles supported on carbon. However the use of palladium as the metal core still has the disadvantage of high price. The objective is to develop a cost effective method that will improve the utilization of Pt while increasing the catalysts activity and durability through alloy formation.

Non-precious metal catalysts have been proposed for the replacement of platinum in low temperature fuel cells, however the low mass activity and low stability have prevents them from being successfully implemented [2]. In order to drive down the cost of fuel cells, while keeping the activity and stability of the catalyst high, active transition metal cores coated with platinum and platinum alloy monolayer were be prepared. The use of an active core will be beneficial in the case when an imperfection in the monolayer exposes a section of the metal core. This process will create a low cost, easy scalable catalyst.

The carbon support was first activated with nitric acid. In this process the carbon surface is oxidized, forming quinone and other oxide groups that will improve the anchoring and dispersion of the metal nano-particles on the carbon surface. Once activated, a transition metal salt such as cobalt nitrate or iron nitrate precipitated on the surface using homogeneous deposition precipitation (HDP) by urea hydrolysis [3]. This method ensures uniform catalyst dispersion and a narrow particle size distribution of 8 nm at metal loadings in the range of 40 wt%.

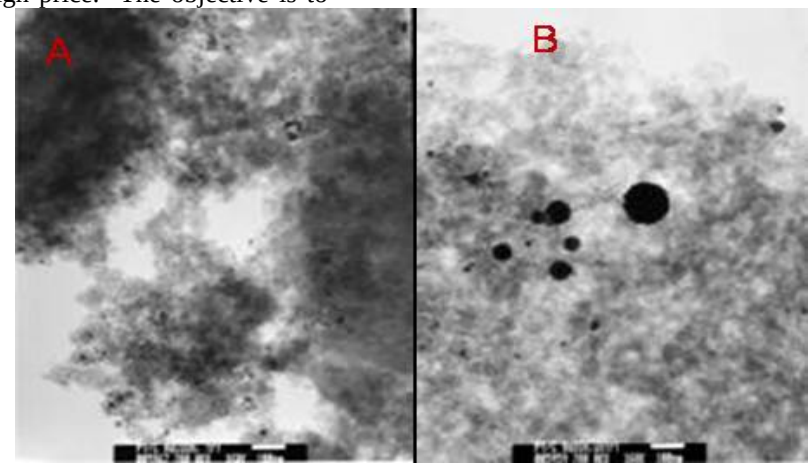

Figure 1: Effect of carbon support pretreatment on Pt particle size deposited under weakly basic conditions, scale is 100nm. (A) HNO_3 treated carbon (B) untreated carbon

The transition metal core was prepared by two different basic conditions that will yield similar particle size, but different oxidation levels. This was controlled by the use of a strong ($NaBH_4$) and weak (NaCOOH) base. The purpose of using two different pHs was to study the effect of the metal core oxidation state on the deposition and activity of the noble metal monolayer. The transition metal salt was precipitated on support by forming insoluble metal chelates on the carbon surface (chelate) [4]. After heat treatment similar particle size distribution and dispersion will be obtained.

The galvanic displacement deposition of Pt was performed at basic and acidic solutions and at 80^{o}C in order to control the deposition/dissolution rate. During the acidic deposition noble metal chloride salts (H_2PtCl_6) was be used and during the basic deposition noble metal hydroxides (e.g. $Na_2Pt(OH)_6$) was be used. Depending on the valence of the platinum group metal salt, for each Pt metal group atom deposited one to two atoms from the transition metal core is dissolved. By using a basic deposition bath the dissolution of the metal core by the acid can be avoided.

Rotating ring-disk electrode (RRDE) provided data on the kinetics of the reaction at the cathode. Since the oxygen reduction reaction is kinetically slow, the data received from the RRDE is vital to understanding how the catalysts will perform when utilized in a membrane electrode assembly for a PEMFC. The RRDE outputs a current-voltage reading during the catalyst reaction with 0.5M H_2SO_4, which can be used to determine the potential for ORR [5, 6]. The additional Pt ring in the electrode is used to determine oxidation that occurs due to H_2O_2 production.

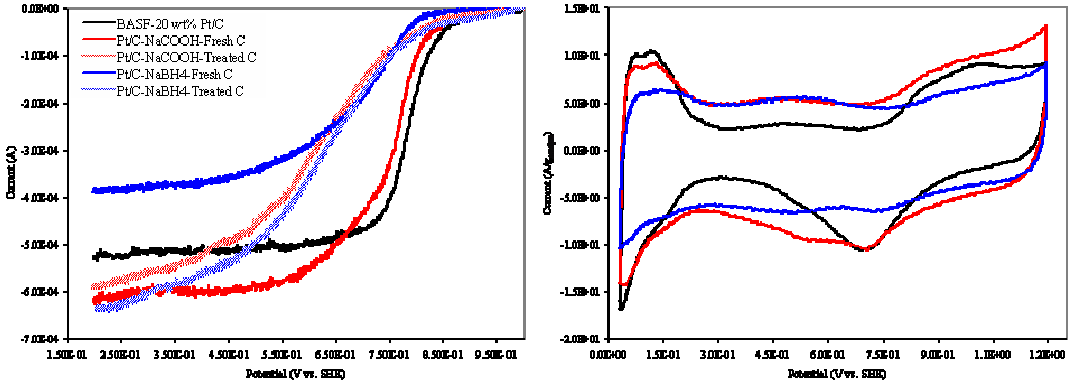

Figure 2: Linear sweep at 800 rpm and cyclic voltagram for catalysts treated with NaCOOH and $NaBH_4$ as compared to a BASF catalyst.

Several findings occurred as a result of this work. A new method for the production of high activity Pt catalysts with reduced Pt loading was explored using Co particles as both the core of the Pt particles and nucleation sites for Pt deposition. It was determined that the Co addition has a higher impact on catalyst when used with $NaBH_4$ as reducing agent as compared to NaCOOH. It is preferred to chemically reduce the Co particles by adding a reducing agent prior to addition of Pt salts. However results indicate incomplete Co reduction may be occurring. The resulting Pt nanoparticles deposition by the galvanic dissolution of Co on the support helps form catalysts with higher activity and surface area.

References:

1. Vukirovic, M. B.; Zhang, J.; Sasaki, K.; Nilekar, A. U.; Uribe, F.; Mavrikakis, M.; Adzic, R. R., *Electrochemica Acta* **2007,** 52, 2257-2263.
2. Atanasoki, R. T. In *Novel Approach to Non-Precious Metal Catalysts*, 2007 DOE Hydrogen Program Review, Washington, DC, May 15-18, 2007, Washington, DC.
3. Bezemer, G. L.; Radstake, P. B.; Koot, V.; van Dillen, A. J.; Gues, J. W.; de Jong, K. P., *J. Catal.* **2006,** 237, 291-302.
4. Subramanian, N. P.; Kumaraguru, S. P.; Colon-Mercado, H. R.; Kim, H.; Popov, B. N.; Black, T.; Chen, D. A., Studies on Co-based catalysts supported on modified carbon substrates for PEMFC cathodes. *J. Power Sources* **2006,** 157, 56-63.
5. Soderberg, J. N.; Sirk, A. H. C.; Campbell, S. A.; Birss, V. I., Oxygen reduction by sol-gel derived Pt/Co- based alloys for PEM fuel cells. *J. Electrochem. Soc.* **2005,** 152 (10), A2017-A2022.
6. Gasteiger, H. A.; Markovic, N. M.; Ross Jr., P. N., H_2 and CO electrooxidation on well-characterized Pt, Ru, and Pt-Ru 2. Rotating disk electrode studies of CO/H_2 mixtures at 62^oC. *J. Phys. Chem.* **1995,** 99, 16757-16767.

High Performance Catalyst Support Materials for Fuel Cells

Hector Colon-Mercado, Mark Elvington, David Hobbs

Objective: Develop a high performance carbon-based catalyst support with significantly improved corrosion resistance.

High surface area carbon serves as the standard catalyst support material for proton exchange membrane fuel cells. This material shows good stability under normal operating conditions, but suffers significant degradation at the cathode when polarized during startup/shutdown cycles. Carbon corrosion results in fuel cells with operational lifetimes well below those required for both stationary and transportation applications. To overcome these limitations, high performance catalyst supports must have the following properties:

- Corrosion resistant – exhibit less than 30 mV decay in performance for a minimum of 200 h operation at 1.2 V, 95 °C, 80%RH, H_2/air,
- High surface area (>100 m^2/g Pt),
- Maintain high electrical conductivity,
- Favorable to load Pt and Pt alloys (30 – 50 wt%), and
- Enhanced metal-support interaction to decrease migration of Pt and Pt alloy.

In this project new catalyst supports containing titanium dioxide (TiO_2) or monosodium titanate (MST) were synthesized via multiple synthetic approaches using two different high surface area carbon powders as base materials: Vulcan XC-72R (Cabot), and Ketjen EC-600 (Akzo-Nobel). These base carbon supports were used as is and also activated by two different methods: (1) sonication in H_2SO_4/HNO_3 and (2) refluxing in HNO_3.

Surface coating of the carbon support with titania proceeded via two methods. The first method consisted of hydrolyzing $TiCl_4$ dissolved in dilute HCl in the presence of the carbon support and PEI (polyethylene imine). PEI is added to promote $TiCl_4$ hydrolysis and stabilize surface bound TiO_2. $TiCl_4$ and carbon ratios were varied to generate coatings of varying densities (i.e. lightly coated/heavily coated). The second method consisted of adapting the synthesis of MST using $Ti(OC_3H_7)_4$ in the presence of the carbon support and $NaOCH_3$. This reaction results in a surface coating of MST which is potentially a more conductive TiO_2 coating with higher surface area.

Platinized carbon powders were prepared by heating a solution of H_2PtCl_6 with dilute NaOH in ethylene glycol at 160 °C. Controlling pH is critical since it controls the glycolate anion concentration which acts as a surfactant for controlling Pt particle size. Pt-colloids are subsequently sonicated with TiO_2 coated carbon in H_2O for 24 h.

Surface morphology of the modified carbon powders (with and without Pt) was evaluated by TEM. Analysis shows surface coverage and TiO_2 structure is dependant on the coating density. The TEM for lightly coated TiO_2 on carbon (dark grey in appearance) shows a well dispersed TiO_2 coating (Figure 1A), whereas the heavily coated TiO_2 on carbon (white in appearance) shows complete TiO_2 surface coverage and the formation of TiO_2 crystals (Figure 1B).

Figures 1C and 1D are TEMs for platinized TiO_2 coated supports for lightly and heavily coated respectively. In general, platinization results in good Pt dispersion with an average Pt particle size of ~5 nm and limited Pt conglomeration. Analysis of lightly coated TiO_2 on carbon (Figure 1C) indicates platinum preferentially deposits onto carbon rather than TiO_2, however platinum will deposit onto TiO_2 when carbon is not exposed on the surface, i.e. heavily coated TiO_2 on carbon (Figure 1D).

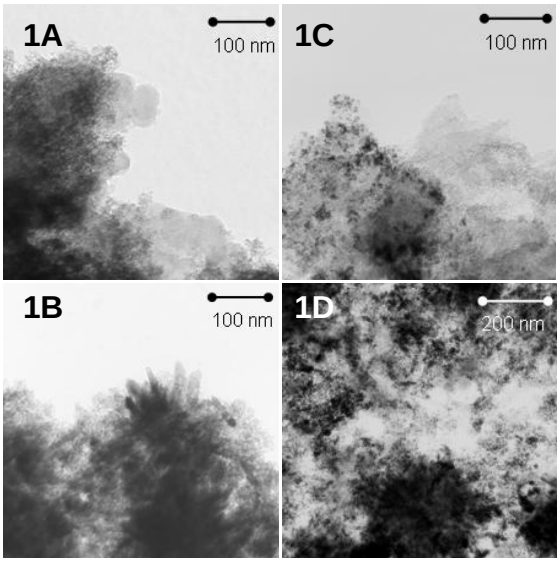

Modified carbon powders (with and without Pt) were screened by TGA for increased oxidative stability. Analysis indicates TiO_2/MST coatings result in increased oxidative stability. Platinized powders display increased oxidative stability but only for TiO_2 coatings with full surface coverage, i.e. heavily coated TiO_2/MST on carbon. TGA analysis indicates 40-50 wt% Pt loading on all samples.

The effect on the conductivity of the supports was tested in a membrane electrode assembly (MEA). Impedance measurements show the lightly coated TiO_2 support to have a resistance of 66 mΩ, which is typical for a hydrogen fuel cell MEA. The heavily coated TiO_2 support was also found to have an acceptable resistance of 103 mΩ. Thus, the TiO_2-coated carbon powders are promising candidates for increased oxidative stability in fuel cells compared to the currently available catalyst support materials. Future plans are to test these materials for oxidative stability under fuel cell conditions.

Ionic Liquid Electrochemical Separations

T. M. Adams, M. J. Williamson, A. E. Visser, and N. J. Bridges

- *This program is focused on evaluating the use of Ionic Liquids (ILs) as electrolytes and solvents for advanced low temperature electrochemical separations processes. The primary focus for this work is related to the development of a fundamental understanding of the electrochemical redox potentials of ILs with a complementary effort to understand the radiation stability of the ILs and the consequences on the electrochemical processes. Experimentally this data is used to deposit metals with large reduction potentials.*

As a result of renewed interest and funding, increased attention is being given to the development of advanced/alternative spent nuclear fuel recycling technologies. The final report from the recent BES workshop on Advanced Nuclear Energy Systems notes that. "*Closing the fuel cycle will create new needs for advanced separation techniques. One possibility is electrochemical separation in (inorganic) molten salts ("pyroprocessing"). A second possibility is the development of a variety of neoteric agents that have the potential to confer unprecedented capabilities for separation of spent fuels in continuous processes, which meet the competing demands of utilizing nuclides formerly considered waste while providing a composition radioactive enough to deter theft and proliferation* and*…With the development of powerful new separation agents, complementary efforts are needed to understand, at a mechanistic level, the consequence on the separation processes of the substantial radiation fields from radioactive decay."* The use of Ionic Liquids (ILs) as an advanced electrolyte for an electrochemical separations process could potentially provide the path for combining the two aforementioned possibilities into a single point operation. The use of ILs in place of high temperature molten salt electrolytes for fuel reprocessing would facilitate operation at lower temperatures and can eliminate many of the technical, environmental, and safety concerns related to high temperature pyrochemical processing. Additionally, the ability to tailor the properties of IL solvents holds the promise of purifying and recovering actinides. For room-temperature electrochemical techniques for use of ILs in an advanced low temperature electrochemical separations process, major emphasis must be placed on development of a fundamental understanding of the electrochemical redox potentials, the radiation stability of the ILs and the consequences on the electrochemical processes from radicals and intermediate decomposition products formed as a result of radiation.

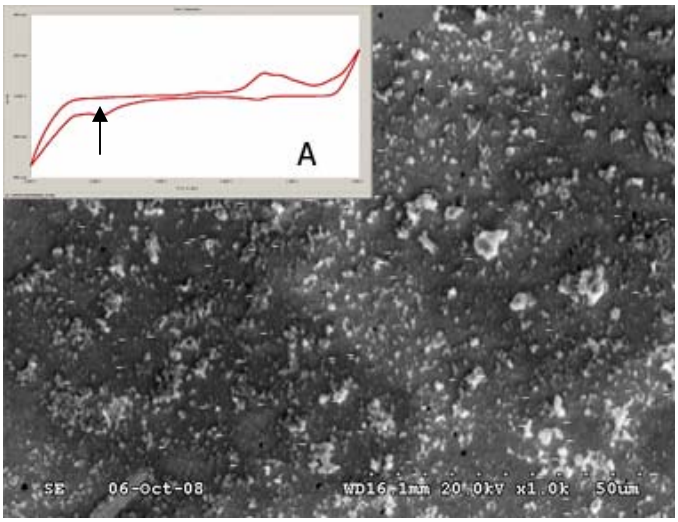

Figure 1:EDX image of Au electrode post Ce deposition. Inset A is CV of IL/Ce salt solution deposition was performed at -2.2V, (arrow).

In FY08, SRNL expanded previous work to evaluate seven commercially available ILs for potential application in electrochemical separations processes. Testing of these materials focused on evaluating of the electrochemical stability of the ILs through cyclic voltammetry (CV), which was used to define the potential range where reduction or oxidation of the IL did not occur. This work as well as FY07 results of irradiation testing were used to select candidate ILs for experiments designed to plate metals with large reduction potentials similar to uranium. Salts of cerium, zirconium, and uranium as well as several ligands were added to the selected ILs. Chronocoulometry experiments were conducted to plate the metals.

Results form the both the cyclic voltametry and plating experiments are as follows:

- Major challenge to replace high temperature molten salts with ILs for pyroprocessing is salt solubility.
- Plating of Cerium was demonstrated while that of Zr and U were not plated.

The current experimental program focused on the thermodynamics of plating and demonstrated that ionic liquids are fully capable of acting as both solvent and electrolyte for electrochemical separations. It is however necessary to match the separation with the IL and further studies are required for determining a process for electroplating Zr and U. Focus should be placed on metal dissolution in the electrolyte.

Life Span of Novel Biopolymer Sequestering Agents for Organic and Inorganic Contaminants

A.S. Knox, C. E. Turick, and M. H. Paller

Objective: The main objective of this project was to develop cross-linked biopolymers that remove contaminants and resist biodegradation over long periods of time.

This research contributes to Goal 1 – leading the DOE for the reduction of technical risks and costs for cleanup – by evaluating the suitability of novel biopolymers for long-term remediation of contaminated soils and sediments.

Biopolymers are high molecular weight compounds with repeated sequences that contain multiple reactive sites with potential to chemically interact with other compounds. Cross-linking agents added to biopolymers enhance their strength and decrease their biodegradability. Previous research suggests that cross-linked biopolymers are stable in soil, and that stability may increase over time, in some cases entrapping contaminants in stable geopolymers. However, the stability of biopolymers and their life span in the field may be affected by environmental conditions indicating a need for further evaluation before this technology is used for remediation. We evaluated the stability of selected cross-linked biopolymers over extended periods (10 weeks to 6 months) in the laboratory. Temperature and leaching studies simulated accelerated weathering. Indications of degradation or loss of effectiveness served to identify potential concerns with long-term stability.

Our research showed that cross-linked biopolymers suitable for soil remediation can be economically produced from commercially available materials. These cross-linked biopolymers sequestered a variety of metals (e.g., As, Cd, Co, Cr, Cu, Ni, Pb, and Zn) and organic contaminants (Fig. 1 and Table 1). Removal of most metals exceeded 90% (Fig. 1).

A ten week evaluation of several biopolymers showed that chitosan cross-liked with guar gum and borax (CGB) and xanthan cross-linked with chitosan and calcium chloride (XCc) had the lowest release of CO_2; i.e., the lowest degradability (Fig. 2). Biopolymers, especially xanthan cross-linked by guar gum, degraded faster under wet conditions and high temperatures (35°C), than under dry conditions (Fig. 3).

Table 1. Average sorption coefficients of sand and sand coated by biopolymers (standard deviation in parentheses); B - borax, C - chitosan, G - guar gum, X - xanthan, c - calcium chloride.

	Phenanthrene L kg^{-1}	**Pyrene L kg^{-1}**
Sand	**3.19** (1.87)	**27.01** (5.34)
CGB & sand	**40.64** (24.32)	**118.3 (17.15)**
XCc & sand	**12.8** (3.42)	**106.7** (15.08)

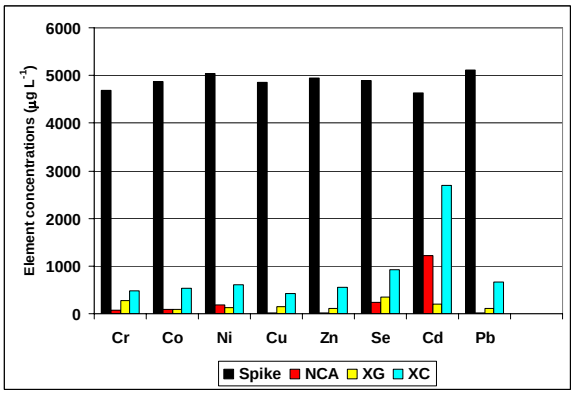

Figure 1. Removal of metals by biopolymers from a spike solution with an initial concentration of 4800 µg L^{-1} of As, Cd, Co, Cr, Cu, Ni, Pb, Se, and Zn; NCA - North Carolina apatite, XG - xanthan cross-linked with guar gum, XC - xanthan cross-linked with calcium chloride.

Microbial densities associated with the polymers were likely a result of bacteria present during manufacture of the polymers. Minimal increases in bacterial densities and CO_2 release over 6 months (Figs. 2 and 3) and under various conditions (Fig. 4) indicated that polymer-associated microbes did not contribute significantly to polymer degradation.

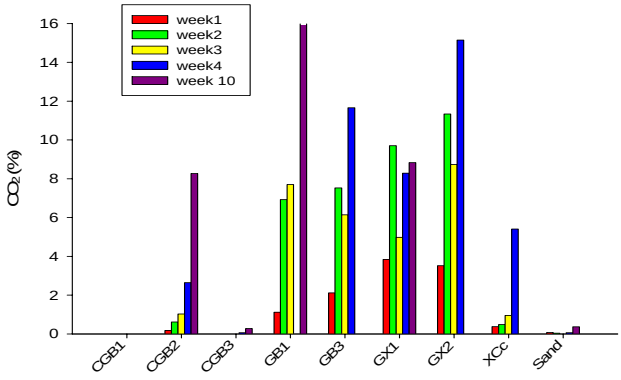

Figure 2. Release of CO_2 (measured by GC-MS) from several cross-linked biopolymers; B - borax, C - chitosan, G - guar gum, X - xanthan, c - calcium chloride, 1 & 3 - without glutaral-dehyde, 2 - with glutaraldehyde, 3 - with NaOH.

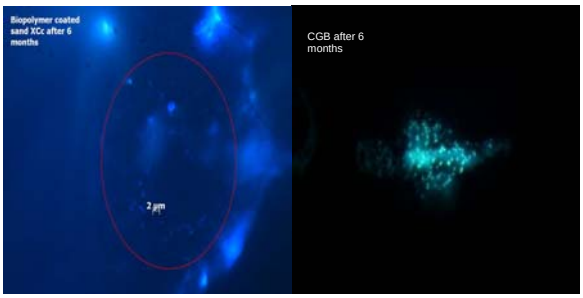

Figure 3. Microscopic analyses of biopolymer surfaces using 4',6-diamidino-2-phenylindole (DAPI) and epifluorescence microscopy. Biopolymer XCc (left) contained fewer bacteria than CGB after 6 months of contact with sediment suggesting limited biodegradation.

Biopolymers with sorbed metals demonstrated decreased CO_2 release and likely minimal biodegradation compared to biopolymers without sorbed metals (Fig. 4). Obvious morphological differences in bacteria isolated from biopolymers indicated that the metal concentration affected the microbial consortia associated with the biopolymers. Biodegradation of biopolymers resulted in minimal release of metal contaminants (Fig. 5).

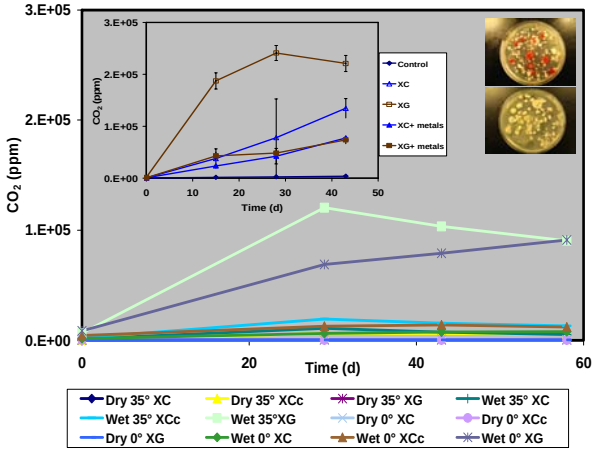

Figure 4. Evaluation of biopolymer degradation without added bacteria, under wet/dry conditions and different temperatures; X - xanthan, G - guar gum, C-chitosan, c - calcium chloride. Inset, (left); CO_2 release after addition of a bacterial inoculum from sediments. Metal sorption of biopolymers inhibited bacterial activity. Inset (right); Morphological differences in bacterial populations after exposure to Xanthan polymers without (top) and with (bottom) sorbed metals.

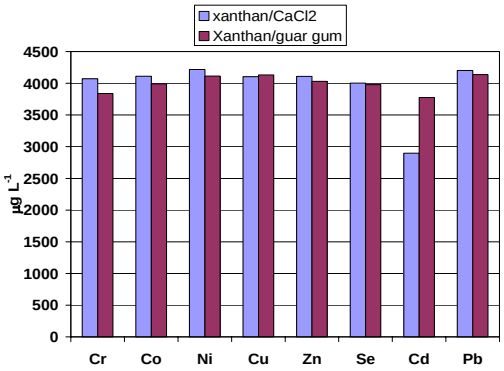

Figure 5. Metals remaining in biopolymers after 3 months of biodegradation (initial concentration of the spike solution was 5000 μgL^{-1}).

This study showed that cross-linked biopolymers have the potential to remove contaminants from the aqueous phase and to stabilize contaminants in soils/sediments. Cross-linked biopolymers vary in their susceptibility to biodegradation, with some being resistant for several months. Biopolymer degradation did not result in contaminant release during the test period. Our research showed that cross-linked biopolymers are promising for remediation; but longer periods of evaluation are still needed.

Novel Electrochemical Process for High Capacity Energy Storage

Brenda Garcia, Josh Gray, Ted Moytka, and Ragaiy Zidan

Objective: Our aim is to produce high hydrogen content compounds that can be used for energy storage and/or battery electrodes. Our effort utilizes a novel method of forming alane (AlH_3) complexes, based on the fundamental thermodynamic characteristics of materials and electrochemical techniques. The research work on this project is expected to address energy storage and battery targets such as system gravimetric and volumetric energy densities, cost and longevity.

Discovering efficient and economic energy storage and battery electrode materials with higher energy density is a critical issue for creating lighter, cheaper energy storage and battery systems. The DOE is supporting research to develop new high energy density and electrode materials with specific objectives of developing more robust systems for long range transportation applications. Researchers have identified large number of hydride materials with high energy densities that can meet the DOE goal of 100 Wh/kg energy density for batteries. Unfortunately, the majority of these compounds fail to fulfill the thermodynamic and kinetic requirements for electrochemical generation. However, alane (AlH_3) not only has the needed gravimetric and volumetric energy density. On the other hand, two problems with using AlH_3 for electrode reactions are the initial generation of AlH_3 and keeping AlH_3 stable in solution. Direct hydrogenation of aluminum to form AlH_3 requires 10^5 bars of hydrogen pressure at room temperature. These extreme hydrogenation conditions had precluded AlH_3 from being considered as a hydrogen storage material in the past. Alternatively, as a part of the DOE hydrogen storage program we were successful to reversibly produce alane electrochemically. Our research work is focused on developing a novel electrochemical technique that can cost effectively generate alane and other high capacity hydrides under practical conditions. One of these high capacity materials is Triethylenediamine-Alane (AlH_3-TEDA) which we used as a complexing agent to prevent alane from decomposition in solution.

For battery applications, amine complexes (e.g. TEDA) are favored to stabilize alane and protect it from decomposition in solution. Alane is an attractive candidate with gravimetric capacity of 10 wt% and volumetric capacity of 149 g/L H_2 and desorption temperature of ~60^{o}C to 175^{o}C (depending on particle size and use of catalyst). The gravimetric hydrogen storage capacity of alane is reduced by forming AlH_3-TEDA complexe, but the complex is more stable in solution and allows the energy storage or battery charging system to be achieved under ambient conditions. AlH_3-TEDA complexes have a gravimetric hydrogen storage capacity of 2.1 wt%, while traditional $LaNi_5H_6$ and mishmetal metal Nickel hydride electrodes store less than 1 wt% hydrogen.

Cyclic volummmetry (CV) was conducted and the regions of voltage needed to form alane-TEDA complex were identified. The oxidation of aluminum to alane was found to occur at -1.63 V vs. SHE. This equilibrium potential can be seen in the cyclic voltammagram in Figure 1 where the current is zero. This is close to the -1.57 V equilibrium potential calculated for the reaction using thermodynamics. During the electrochemical reaction, the white AlH_3-TEDA complex precipitate was formed at the aluminum anode as shown in Figure 2. The white precipitate formed at the aluminum electrode was identified by XRD as AlH_3-TEDA as shown in Figure 3. XRD comparison of the electrochemically formed A1H3- TEDA complex to a standard sample of A1H3- TEDA complex prepared by a chemical method.

Other fellow researchers have synthesized AlH_3-TEDA using a chemical synthesis route, which utilizes Ti-activated aluminum which is charged with H_2 in THF in the presence of TEDA. However, with the novel electrochemical route that is reported here, pure aluminum electrodes are employed to precipitate AlH_3-TEDA from solutions of $NaAlH_4$ in the presence of TEDA, which electrochemical charging times are typically less than one day. These times could be theoretically reduced for a given amount of AlH_3-TEDA product by utilizing large industrial size electrode assemblies. After the AlH_3-TEDA is separated from the electrolyte solution, it is then activated using a simple ballmilling technique with $TiCl_3$. The reversibility of the

electrochemically synthesized AlH_3-TEDA was verified using a Sievert's type apparatus. The material can be discharged at the relatively moderate temperature of 80 ^oC; however, of more importance is the fact that the material is recharged at room temperature with a pressure of 70 bar (well below the pressure of a standard laboratory-grade gas cylinder.)

This work shows promise of developing new battery technologies, using a higher capacity metal hydride complex for rechargeable battery applications. The hydride was synthesized using an electrochemical technique which was designed to avoid the need to pre-activate the aluminum material to reduce the time scale required for synthesis. Furthermore, a battery based on this technology can be recharged using an off-board supply of relatively low pressure H_2 gas at room temperature.

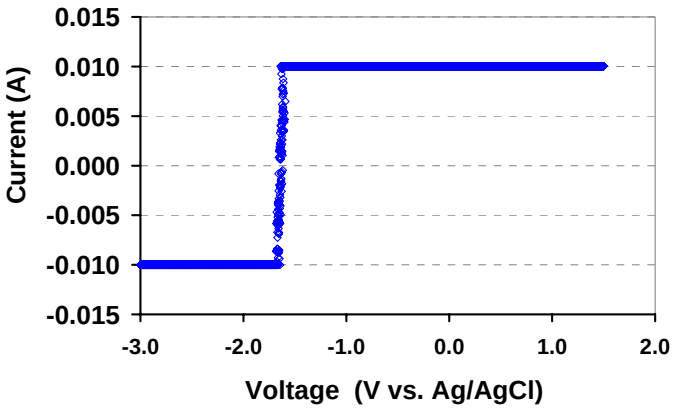

Figure 1. CV of the aluminum working electrode in the alane generation cell

Figure 2. TEDA-Alane formation during the electrochemical reaction

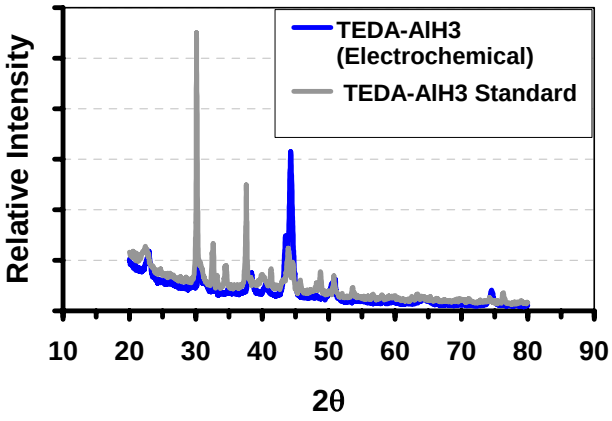

Figure 3. XRD comparison of the electrochemically formed $A1H_3$-TEDA complex to a standard sample of $A1H_3$- TEDA complex prepared by a chemical method.

Novel Nanostructured Anode Materials for Li-Ion Rechargeable Batteries with High Capacity and Inherent Safety

Ming Au

This project aims to grow free standing metal oxides and metals nanostructure as the high capacity anode for Li-ion rechargeable batteries. Using hydrothermal deposition process, the free standing Co_3O_4 nanorods has been successfully grown on titanium substrate confirmed by SEM (Scanning Electron Microscope) (Fig.1-2) and XRD (X-ray diffraction) (Fig.3).

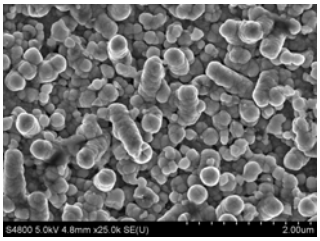

Fig.1 Co_3O_4 hollow nanorods grown on Ti substrate (X25,000)

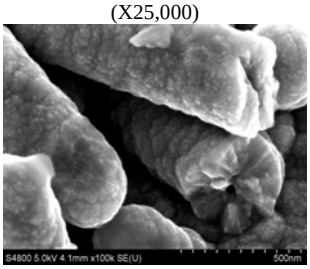

Fig.2 Co_3O_4 hollow nanorods grown on Ti substrate (X100,000)

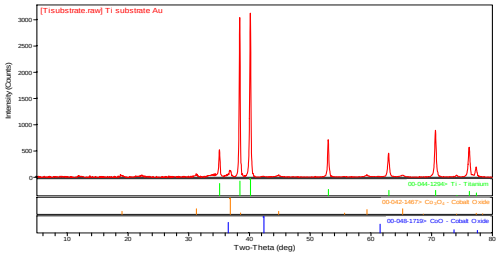

Fig.3 XRD of Co_3O_4 nanorods thin film on Ti substrate

The free standing Co_3O_4 nanorods were used as anode directly without any additives and binders. The electrochemical evalyation shown that Co_3O_4 nanorods – Li cell delivered 1300 mAh/g reversible capacity (at high rate of 2.76 A/g) that is four time higher than carbon base anode (370 mAh/g) used by today's Li-ion rechargeable batteries (Fig.4).

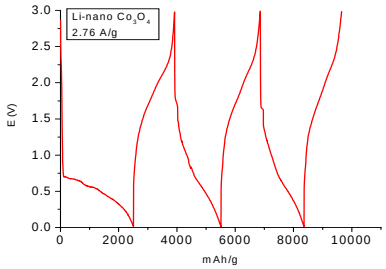

Fig.4 The charge-discharge cycle of a half cell made by Co_3O_4 nanorods and Li

In the second part of this project, the aligned Aluminum nanorods were grown on Ti substrate by glancing angle deposition (Fig.5). The aligned Al nanorods were used as the anode directly in an electrochemical cell without additives and binders. The Al nanorods – Li cell demonstrated 1243 mAh/g reversible capacity (Fig.6).

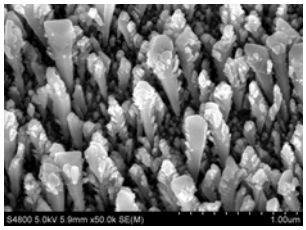

Fig.5 Aligned aluminum nanorods (x50,000)

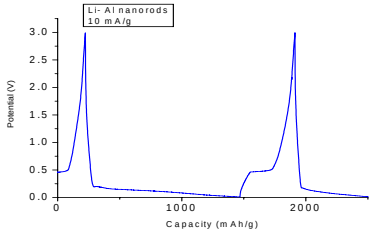

Fig.6 The charge and discharge behavior of a half cell made by Al nanorods and Li

Our experimental results prove the concept proposed in this LDRD project:

The free standing nanostructured metal oxide and metals offer high energy density and power density with inherent safety even at very high charge and discharge rates.

Rate of Eutectic Formation in Plutonium-Stainless Steel Couples

Philip E. Zapp, Andrew J. Duncan and Robert A. Pierce

Iron can react with plutonium in what is termed a eutectic reaction to form a two-phase solid mixture that is in equilibrium with a molten plutonium – 10% iron solution at a temperature more than 200°C lower than the 640°C melting point of pure plutonium. As seen in Figure 1, the melting temperature of plutonium – iron alloys decreases continuously from 640°C to 410°C with increasing iron concentration from zero to 10%. Plutonium iron alloys with iron concentrations ranging up to 10% may form by diffusion of iron into plutonium. (The reverse flux of plutonium into iron is negligible because the diffusion coefficient of the much larger and heavier plutonium atom into iron is much lower than that of iron into plutonium.) With sufficient diffusion of iron and at temperatures greater than 410°C, a molten plutonium – iron phase may form within a solid plutonium matrix.

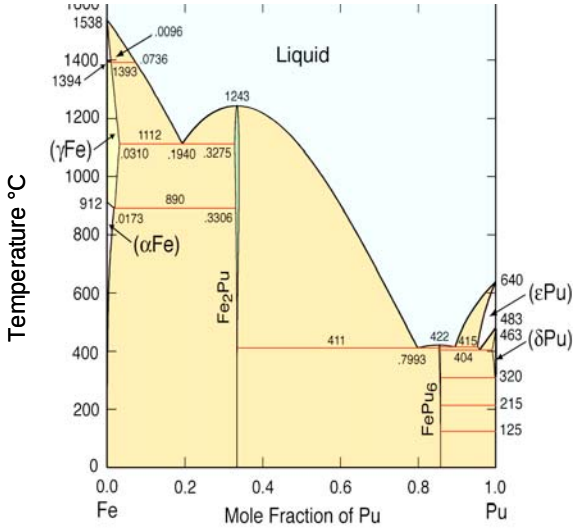

Figure 1. Plutonium – iron phase diagram.

In Department of Energy facilities, plutonium is held in containers fabricated from austenitic stainless steels, alloys of iron, chromium, and nickel with a face-centered cubic crystal structure. (Nickel also reacts eutectically with plutonium; chromium does not.)

Such containers can serve as the source of iron (and nickel) that can diffuse into plutonium at elevated temperatures. The containers themselves may be structurally degraded should they be contacted by molten plutonium – iron or plutonium – nickel alloy. Thus the rate of eutectic alloy formation is of interest in assessing the performance of plutonium containers under elevated temperature conditions. The rate of formation depends on the actual diffusion of iron or nickel into plutonium. Both plutonium and stainless steel are readily oxidized in air, so that surface oxides on each can be expected to reduce the diffusion rates. Beyond the uncertain effect of oxides on diffusion rates, the diffusion coefficient itself of iron in plutonium is not well known.

Preparations were completed to conduct the eutectic formation experiments. Delta-phase plutonium wafers were shipped from Los Alamos National Laboratory to SRS on September 22, 2008. A glovebag has been fabricated that will be used to cut samples from the wafers under a nitrogen atmosphere. Fixtures for the heat-treatment of the plutonium-stainless steel couples have also been fabricated. Follow-on funding will be sought to carry out the experiments.

Real-Time Airborne Beryllium Particulate Monitor

C.J. Coleman, B.B. Anderson, R.K. Huffman, A.G. Harter, D.J. Pak

The goal of this research was to support the DOE Environmental Management mission by developing a compact monitor to detect trace levels of airborne beryllium particulates in the environment. The concept tested was integration of the Aerosol-to-Liquid Particle Extraction System (ALPES) developed by the Savannah River National Laboratory with the fluorescence detection method developed by the Los Alamos National Laboratory and licensed commercially to Berylliant.com. The ALPES was a winner of the *R & D Magazine* award for one of 100 best new technologies in 2003. The system draws up to 300 liters/minutes of air past a corona charging section for particle deposition on the charged, wetted surface of the standpipe. Capture of the particles into liquid has advantages over collecting the particles onto a filter. Liquid capture permits, after development of a suitable pumping and control system, transfer of the particles directly into the fluorometer for detection. Since the fluorometric method is sensitive to 0.005 μg beryllium, the integrated ALPES/fluorometric monitor would provide a sensitive and convenient automated system for monitoring the environment for airborne beryllium particulate contamination. The monitor would include and alarm system for alerting workers that airborne beryllium contamination has been detected. Potential applications of the monitor include industrial hygiene surveillance of DOE and industrial operations and decontamination and decommissioning work in beryllium-contaminated facilities.

An ALPES was fabricated and tested for particulate collecting efficiency. Efficiency tests were performed by placing the ALPES in a polycarbonate containment box with the dimensions of 60” wide x 36” deep x 42” high. An ultrasonic nebulizer was used to spray a mist of NaCl that upon evaporation created particles with diameters in the range of 0.1μm-3.0 μm. An optical particle size detector was used to measure the particle size change induced by ALPES collection from which the efficiency was calculated. The ALPES fabricated for this work collected the NaCl particles with an average of 57% efficiency. Because the containment box was not located in a fume hood to permit tests with hazardous beryllium materials, alternative arrangements for performing efficiency tests with beryllium oxide in a fume hood were considered. The powder dispersion equipment intended for these tests was not delivered until after the LDRD period was over. Simple powder dispersion tests were performed but the experimental setup in the fume hood was not adequate for definitive ALPES efficiency tests with actual beryllium oxide powder.

Dissolution tests confirmed that a dilute solution of ammonium bifluoride at room temperature is adequate for dissolving beryllium oxide particles in the size range of concern for inhalation. Room temperature dissolution is important for development of a convenient real-time beryllium monitor. The beryllium oxide material used in the tests was a new Certified Reference Material created by a collaboration of the National Institute for Standards and Technology, SRNL, and two other laboratories.

An electrical engineering conceptual scheme was developed for ALPES automation and integration with a fluorometer for continuous monitoring of airborne beryllium contamination. A sixteen bit embedded controller with integral time/date clock and nonvolatile memory will be the main system controller to keep the monitor system as compact and portable as possible. An interface port on the system will retrieve stored data from the ALPES system, perform diagnostic testing, and modify key operating parameters, such as fill levels and alarm points. The embedded controller will interface directly to associated sensors for monitoring liquid levels, voltages, and other pertinent operating parameters. In instances where there is a potential for high voltage to infiltrate sensor lines, isolation will be employed to protect the embedded controller and other sensitive electronics. Interface requirements for the fluorometer will be application specific and these requirements will be elucidated with laboratory tests. ALPES capture liquid transfers will be achieved through the step function control of meter pumps, continuous duty pumps with external level sensors, or pulse-width modulated controlled pumps. The application board will contain the embedded controller, interface components, DC power regulation circuits, and time/date clock battery. The embedded system application board will contain a wide range DC-

to-DC converter to allow embedded controller interface with pumps and other DC components. User interface will be provided through either dedicated indicators, audible alarms, text displays, or a combination of these to yield a user-friendly monitor system.

The basic concept of collecting hazardous airborne particulates with the ALPES followed by automated transfer of solution to a detector has applications beyond beryllium detection. Integration of the ALPES with nuclear counting equipment will allow airborne radionuclides to be collected and transferred to liquid scintillation or other counting equipment for measurement. Development of an integrated ALPES/liquid scintillation system for real-time detection of airborne metal tritide contamination in SRS Tritium Department facilities was selected as a winning Plant Directed Research and Development proposal for FY 2009.

Separation of the Transuranic Actinides from the Lanthanides Using HDEHP

T. S. Rudisill, D. P. DiPrete, and M. C. Thompson

Objective: The objective of this research was to identify a complexant which can be used to replace diethylenetriamine-pentaacetic acid (DTPA) in the TALSPEAK solvent extraction process for the separation of the transuranic actinides from the lanthanides. Partitioning the minor actinides from the lanthanide elements is one of the most technically challenging separations required to support the complete recycle of spent nuclear fuel. The flowsheet under development by the Advanced Fuel Cycle Initiative currently employs the TALSPEAK process to preferentially extract the lanthanide elements into bis-(2-ethylhexyl)phosphoric acid (HDEHP) from (pH 3-4) aqueous phases containing 1.5 M lactic acid and 0.05 M DTPA. The separation is based on the extraction of the lanthanide/lactate complexes and the rejection of the actinide/DTPA complexes to the aqueous phase. However, an efficient separation requires very tight control of the aqueous phase acidity which would likely be difficult to consistently achieve on a large scale. To address this issue, we measured distribution coefficients for lanthanide and transuranic elements between aqueous and organic phases in the presence of alternate complexants to identify replacements for DTPA which improve the feasibility of deploying a modified process on an industrial scale.

Five complexants with the potential to replace DTPA in the TALSPEAK process were tested: acetohydroxamic (AHA), benzohydroxamic (BHA), and salicylhydroxamic acids (SHA), ammonium thiocyanate (NH_4SCN), and N,N,N′,N′ - tetrakis (2-pyridylmethyl) ethylenediamine (TPEN). The extraction experiments were performed by preparing aqueous solutions of each complexant containing lanthanide and actinide tracers. Lanthanide tracers were prepared by activating a stable lanthanide solution in the SRNL Neutron Activation Analysis Facility. The actinide tracers (^{239}Np, ^{238}Pu, and ^{241}Am) were prepared from existing inventories of material. The ^{239}Np tracer was prepared by milking an ^{243}Am source. Extractions with each complexant were performed in triplicate at pH 2, 3, and 4. Distribution coefficients for the lanthanide and actinide elements (D_{Ln} and D_{Ac}) were obtained from the ratio of the activity of each element in the organic (1 M HDEHP) and aqueous phases. The activities were measured by gamma pulse height analysis.

In the initial scouting experiments performed with each complexant, we found that the presence of AHA, BHA, or SHA in the aqueous phase did not prevent the extraction of the actinide elements into HDEHP. The separation factors (D_{Ln}/D_{Ac}) were near unity. In the initial experiments, we also found that distribution coefficients for the extraction of the lanthanide elements into 1 M HDEHP were very large. Little activity remained in the aqueous phase for a number of the lanthanide tracers. Activities near the detection limits resulted in large uncertainties associated with the distribution coefficient measurements. To address this issue, we reduced the HDEHP concentration to 0.125 M to lower the lanthanide extraction. The use of a more dilute concentration improved the precision of the measurements; however, the high solvent loading resulted in third phase formation (primarily at pH 4). Increasing the organic/aqueous (o/a) ratio was generally successful in eliminating the third phase.

In additional experiments using 0.5 M NH_4SCN in the aqueous phase, we found that the actinide separation factors increased with increasing atomic number of the lanthanide elements (Figure 1). The actinide elements exhibit more similar extraction behavior to the "light" lanthanide elements due to the similar size of the ionic radii. When 0.05 M NH_4SCN was present in the aqueous phase, the lower concentration was insufficient to separate the actinides from the lanthanides.

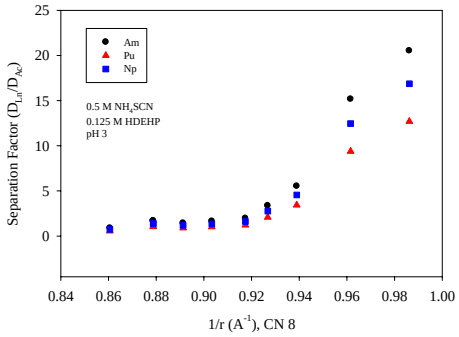

Figure 1 Separation factors for NH_4SCN

Similar extraction behavior (to NH_4SCN) was observed when 0.05 M TPEN was present in the aqueous phase. The actinide separation factors also increased with increasing atomic number of the lanthanides (Figure 2).

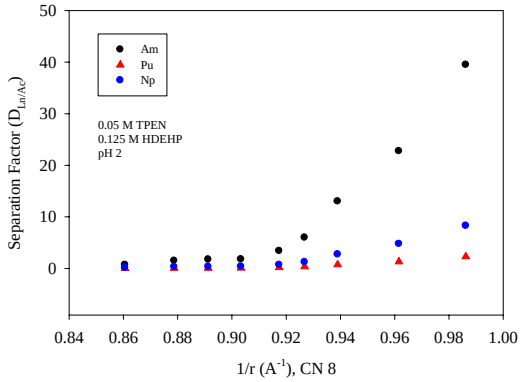

Figure 2 Separation Factors for TPEN

Experiments performed using 0.03 M TPEN did not effectively separate the actinide from the lanthanide elements. Extractions performed at pH 3 and 4 also exhibited third phase formation; however, the third phase was eliminated at pH 3 by increasing the o/a ratio from 1:1 to 2:1.

Extraction experiments were also performed using DTPA in the aqueous phase to confirm that distribution coefficient data generated using our methods are consistent with published literature. In these experiments, separation factors for 0.05 M DTPA were much higher than those measured using either NH_4SCN or TPEN (Figure 3).

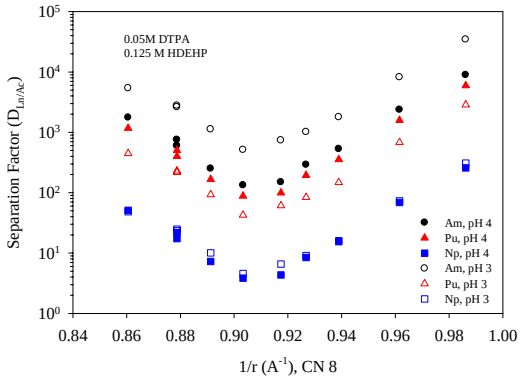

Figure 3 Separation factors for DTPA

The data in Figure 3 also show that the separation between the lanthanides and actinides in the presence of DTPA is minimized at Nd (1/r = 0.903) which is consistent with data published in the open literature. This result provides validation for our distribution coefficient measurement technique. The data also illustrate that none of the complexants that we tested provided better separation of the actinide from the lanthanide elements than DTPA. DTPA is still the complexant of choice for use in the TALSPEAK process. However, our work was successful in developing a rapid and accurate technique for measuring distribution coefficients for actinide/lanthanide separations which may be extremely useful in solving the difficult Am/Cm and Am separation challenges associated with the closure of the nuclear fuel cycle.

Stable Isotope Nitrogen-15 Production

L. K. Heung, H. T. Sessions, W. A. Spencer

Objective: The objective of this project is to research a new process for the production of high purity nitrogen-15 (N-15), a stable isotope of nitrogen. Nitride fuel with N-15 is the fuel of choice for advanced nuclear reactors because it offers advantages in density, thermal conductivity, chemical compatibility, and neutron efficiency. But the cost of N-15 is too high to be economically competitive. A low cost N-15 production process is needed. The goal of this project is to find an efficient separation process so the cost of N-15 can be reduced by a factor of 10, from about $300/g to $30/g.

N-15 exists naturally. Its abundance is 0.366% by atoms. High purity N-15 is produced by extracting N-15 from natural nitrogen or its compounds. Present production methods include chemical exchange such as that between ammonium and nitric acid, and cryogenic rectification of nitric oxide. The complexity of these existing processes is the main cause for the high cost. This project has investigated two potentially simpler methods, the thermal cycling adsorption method and the room temperature fractionation method. Ammonia was chosen to be the raw material because it contains a single nitrogen atom in a molecule ($^{14}NH_3$ and $^{15}NH_3$), is stable and has favorable vapor pressures at near ambient temperatures. Once pure $^{15}NH_3$ is produced it can be easily decomposed and purified to $^{15}N_2$.

SRNL invented and developed a thermal cycling absorption process named TCAP for separating hydrogen isotopes. This TCAP process has been in production service at DOE Savannah River Site for over 12 years and has been performing very well. The premise for this project was that a similar process might also be efficient for separating ammonia-15 ($^{15}NH_3$) and ammonia-14 ($^{14}NH_3$). Application of the TCAP process requires an absorbent that absorbs ammonia reversibly and that has an isotopic effect to ammonia-15 and ammonia-14. Isotopic effect is defined as $\alpha = ([^{14}NH_3] / [^{15}NH_3])_{vapor} / ([^{14}NH_3] / [^{15}NH_3])_{solid}$, where the [ ] is concentration. The value of α must not be one and must be temperature dependant. The first task of the project is to select candidate absorbents and test them for isotopic effect toward ammonia.

Four adsorbents were selected for testing: molecular sieve 5A, molecular sieve 13X, porous polymer HayeSep® C and DOWEX MAC-3. The absorbent were packed in 30-ft long, 2-mm ID stainless steel columns for the experiments. Three types of experiment were devised to detect the isotopic effect of the absorbents: band displacement, step change and thermal cycling. In band displacement, a sample of ammonia is first absorbed in the column and then eluted by flowing helium or nitrogen. A RGA (residue gas analyzer) is used at the outlet of the column to measure concentrations. If there is an isotopic effect the ammonia-14 and ammonia-15 would be separated and exit the column at different times. In the step change experiment, the feed to the column is changed from helium (or nitrogen) to ammonia in a step. If there is an isotopic effect the ammonia-14 and ammonia-15 would show up at the column exit at different times. In both cases the time that separates the exit of the two compounds would be a measure of the separation factor. In the thermal cycling experiment, the packed column is connected to another column that is not packed. The packed column will be heated and cooled between room temperature and 180 °C. The column will absorb and release the ammonia as the temperature goes from cool to hot. The ammonia vapor will be transferred to and from the empty column. The purpose of the empty column is to provide a plug flow volume for the transfer of the ammonia from and to the packed column. The repeated cycling can accumulate the separation that each cycle can produce and therefore amplifies the separation

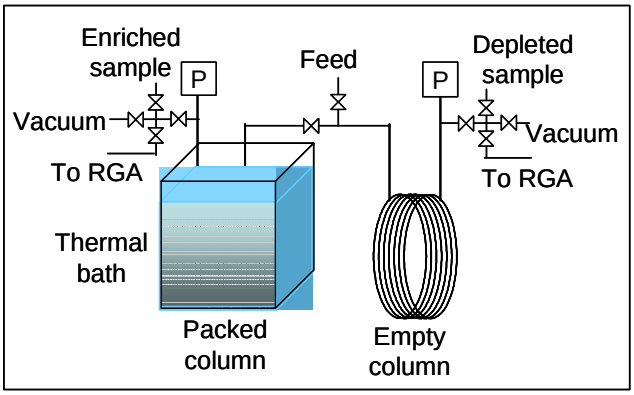

Figure 1. Schematic of thermal cycling absorption experiment.

effect of the packed column (Figure 1). Enriched and depleted samples are collected for analysis in a high resolution mass spec. A typical mass spectrum of ammonia is shown in Figure 2. Note that there are three peaks (18.01 H_2O, 18.02 $^{15}NH_3$ and 18.03 $^{14}NH_4$) are very close to each other. That created a challenge to the analysis particularly when the $^{15}NH_3$ concentration is low.

For the room temperature fractionation experiment, a 4-ft long, 3/8" diameter, 0.035" wall stainless steel column packed with 3-mm diameter glass beads was used. On top of the column is a condenser (4" diameter 2.2 liter)

wrapped with ¼" diameter copper coil chilled with salted water at -15 ^{o}C. At the bottom is a room temperature boiler which is a 4" diameter coil made from 10-ft long 1/8" OD, 0.035" wall stainless steel tubing. When the column is filled with proper amount of ammonia, there will be vapor travel upward and liquid travel downward, creating a continuous contact between the vapor and liquid phases. The heavier component ammonia-15 will be enriched at the bottom of the column.

The experimental results showed the following. The isotopic effects of the absorbents tested were too small to be detected with the band displacement method and the step change method. But the thermal cycling method did show separation of the heavy and light ammonia. Twenty thermal cycles of the molecular sieve 5A column enriched the ammonia-15, changing the $^{14}NH_3/^{15}NH_3$ ratio from 272 (natural abundance) to 188. The room temperature fractionation column showed even better results. The 4-feet column enriched the ammonia-15 to a $^{14}NH_3/^{15}NH_3$ ratio to 130. These results are encouraging but far from being conclusive. Continuous efforts are needed. The room temperature fractionation method in particular is very appealing due to its simplicity and low energy requirement. Its further investigation is strongly recommended.

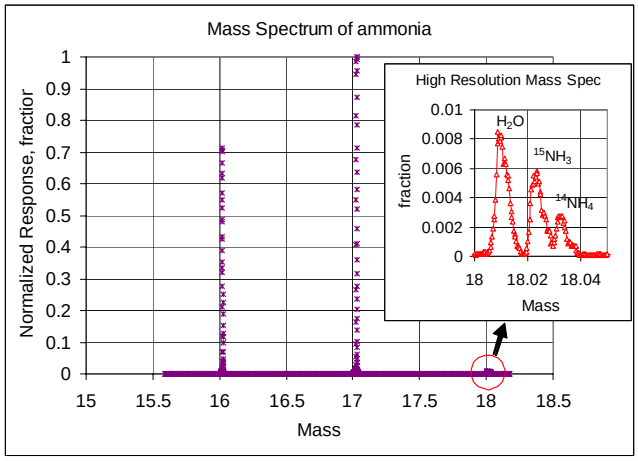

Figure 2. Mass spectrum of ammonia showing the peak of $^{15}NH_3$.

Structural Interactions of Hydrogen with Bulk Amorphous Microstructures

L. Brinkman, E. Fox, P. Korinko, and T. Adams

- *This program is focused on understanding the role of hydrogen induced partial crystallization on the permeation properties of amorphous metallic glass membranes used in commercial hydrogen separation.*

A major focus area of metallic glasses is their use as hydrogen separation membranes to replace the high cost of Palladium Pd/Pd-alloy membranes. An obstacle to their large scale employment in membrane separations processes is the unknown crystallization/devitrification behavior at elevated temperatures and times and subsequent impact on material properties including hydrogen permeation. This project sought to address this fundamental research need by examining the crystallization behavior both structurally as well as the impact on gas transport in these materials.

In order to systematically study the impact of partial crystallization in these materials a variety of compositions were purchased from commercial sources to obtain five Fe, Ni, Co and Zr based metallic glasses. These samples were subjected to Differential Scanning Calorimetry as a function of temperature under different gas compositions in order to quantify phase transition temperature and energies. X-ray diffraction analysis was also performed as a function of temperature and gas composition. Finally, hydrogen permeation properties were measured in two measurement modes i) in-situ where crystallization took place during gas phase hydrogen permeation at elevated temperatures and ii) ex-situ where pre-crystallized sample's hydrogen permeation properties were measured and compared with the as-received amorphous materials at ambient temperature using an electrochemical method.

The temperatures, energy release and structure of crystalline phases as a function of temperature and gas composition were identified by DSC and XRD for the 5 BMG materials. The 2826 alloy was chosen for further kinetic studies due to availability of literature data on kinetic crystallization parameters for comparison. Kinetic rate parameters were obtained from DSC experiments and Avrami kinetic expressions were used to compare experimental crystallization kinetics with literature. Diffusivity values for the amorphous and crystalline samples determined from hydrogen current transients were comparable and the reduction in permeation is thus attributed to reduced hydrogen solubility in the crystalline phase. Experiments looking at "in-situ" crystallization were inconclusive due to scatter in the hydrogen flux data and system off gassing.

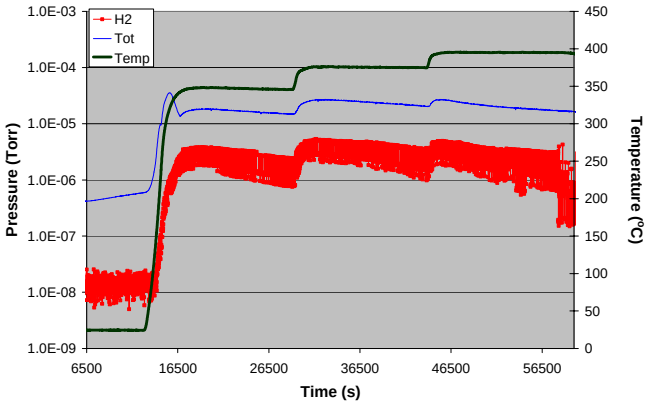

Figure 1. "In-Situ" permeation/crystallization where Pressure and Temperature versus time were measured for 2826 MetGlass membrane in dynamic mode permeation setup. Hydrogen pressure is proportional to hydrogen flux through membrane.

Results from both the kinetic crystallization investigations and the electrochemical and gas permeation are as follows:

- Kinetic crystallization parameters based on Avrami equation were obtained for the 2826 alloy and compared with literature.
- Baseline permeation properties of the amorphous alloys were characterized by i)electrochemical permeation and ii) gas phase permeation.
- The impact of crystallization on the permeation was studied i) ex-situ by annealing samples before measurement and ii) in-situ by measuring gas phase hydrogen permeation during crystallization.
- Ex-situ studies revealed that the hydrogen permeation was reduced in crystalline samples by an order of magnitude from 3 X 10^{-11} (mol H_2/m s) to 2.6 X 10^{-12} (mol H_2/m s) in 2826 alloys due to reduced solubility of hydrogen in the crystalline phase.
- In-situ studies were inconclusive due to the large scanner of the pressure (hydrogen flux) versus time plots in the dynamic measurement mode.

Systems Microbiology for Energy and the Environment: Structural and Functional Analysis of the *Kineococcus radiotolerans* Genome

Christopher Bagwell, Charles Milliken, Chris Yeager - Savannah River National Laboratory
Larry Shimkets - University of Georgia
Kim Hixson, Mary Lipton - Pacific Northwest National Laboratory, EMSL

♦ *Kineococcus radiotolerans* was isolated from a high-level waste environment at SRS yet all we know of this organism concerns its ability to withstand tremendous abuse. The goal of this LDRD continuation was to exploit the genome sequence of *K. radiotolerans* in order to identify potential applications for DOE missions in energy and the environment.♦

Kineococcus radiotolerans was isolated from a high-level waste environment at the SRS in the late 90's. *Kineococcus* is an aerobic, Gram positive, non-pathogenic actinobacterium that belongs to the *Frankineae* suborder of the *Actinomycetales.* Other than the few distantly related species that cause disease, little is known about the *Actinobacteria* or their environmental roles, and our knowledge of *Kineococcus* is restricted to its remarkable ability to withstand DNA damaging agents and cellular assaults. Combined support from SRNL's LDRD program and DOE's Office of Biological and Environmental Research permitted parallel analysis of the *Kineococcus* genomic and proteomic responses to lab simulated contaminated environments. This support has contributed to our understanding of metal metabolism and stress physiology in *Kineococcus*, and now our attention has turned to potential applications for DOE missions in energy and the environment.

The DOE maintains interest in the extreme resistant bacteria for bioremediation because of their ability to withstand the toxicity of contaminated environments. We have shown that the growth and metabolism of *Kineococcus radiotolerans* was significantly enhanced by copper during chronic irradiation. Copper is an essential cofactor for a variety of enzymatic processes; however, at elevated concentrations copper is toxic, thus intracellular levels are tightly regulated by the cell. *K. radiotolerans* was routine grown in medium containing 6 to 95 mg L^{-1} of copper (25 ug L^{-1} is widely considered toxic for environmental bacteria), resulting in intracellular copper accumulation up to 3.7 μg / mg protein without significant retardation in growth. Through detailed physiological experimentation we have identified two concentrations of extracellular copper which significantly stimulates cellular growth and metabolic respiration. The resultant intracellular metal accumulation coincided with protein-level down regulation of specific cellular defense systems. We have collected nearly 1.3 Mb of genome transcriptional information from 454 *FLX* sequencing and recently completed whole cell proteomics analysis of *Kineococcus* at distinct growth stages and in response to copper. Integrated analysis and metabolic reconstruction of these data should shed new light on the fate and function of copper in *Kineococcus*, as well as insights into copper homeostasis networks. Very little is known about the mechanisms for metal resistance in Gram-positive bacteria. Furthermore, it remains unclear why or how copper at such high concentrations stimulates energy metabolism in *Kineococcus*, particularly in a radioactive environment when the combination should be strongly inhibitory to cellular processes.

In the final stages of this LDRD we completed analysis of the the *Kineococcus* genome which was sequenced by the U.S. Department of Energy's Joint Genome Institute. The genome consisted of three distinct replicons, including a linear chromosome, and was examined specifically for ionizing radiation resistance, the potential for bioremediation of nuclear waste, and the dimorphic life cycle. *K. radiotolerans* appears to have a unique genetic toolbox for radiation protection as it lacks many of the genes known to confer radiation resistance in *D. radiodurans*. Additionally, genes involved in the detoxification of reactive oxygen species and the excision repair pathway are overrepresented. *K. radiotolerans* appears to lack degradation pathways for pervasive soil and groundwater pollutants. However, it can respire on two organic acids found in SRS high-level nuclear waste, formate and oxalate, which promote the survival of cells during prolonged periods of starvation. The dimorphic life cycle involves the production of motile zoospores. These results highlight the remarkable ability of *K radiotolerans* to withstand environmental extremes and suggest that *in situ* bioremediation of organic complexants from high level radioactive waste may be feasible.

Bagwell CE, Bhat S, Hawkins GM, Smith BW, Biswas T, et al. (2008) Survival in Nuclear Waste, Extreme Resistance, and Potential Applications Gleaned from the Genome Sequence of Kineococcus radiotolerans SRS30216. PLoS ONE 3(12): e3878. doi:10.1371/journal.pone.0003878

Bagwell CE, Milliken CE, Ghoshroy S, Blom DA. (2008) Intracellular Copper Accumulation Enhances the Growth of *Kineococcus radiotolerans* during chronic irradiation. *Appl. Environ. Microbiol.* 74(5):1376-84.

Understanding Compositional and Kinetic Drivers for Nepheline Crystallization in High-Level Waste Glasses

K. M. Fox, F. C. Raszewski, S. L. Morris, D. K. Peeler

Objective: The strategic goal of this work was to reduce the cost and time necessary for high-level waste cleanup operations by increasing waste loadings in glass. An understanding of the mechanisms of nepheline crystallization will alleviate concerns over durability issues in high waste loading glasses, thus reducing technical risk.

To meet these objectives, a series of test glass compositions was developed for further characterization. The number of components within the glass was greatly reduced from a typical, high-level waste glass. Sodium aluminosilicates were used as the base glass compositions, along with additions of B_2O_3 and CaO. Both B_2O_3 and CaO have previously been shown to hinder nepheline crystallization; however, the mechanisms preventing nepheline formation are not fully understood, nor have they been evaluated in simplified glass systems. Test glasses were fabricated at SRNL using reagent grade chemicals and a high-temperature, resistance-heated furnace. Samples of the glasses were prepared for X-ray diffraction and structural analyses. Portions of each glass were also cooled at varying rates in order to identify the impact of cooling rate on crystallization behavior. SRNL partnered with Clemson University to evaluate changes that occur in the glass structure as the concentrations of B_2O_3, CaO and Na_2O were varied. Various techniques, including Raman and Fourier Transform Infrared spectroscopy, were utilized to determine changes in cation coordination within the glasses.

Significant results of the structure analyses included the observation that as B_2O_3 concentrations were increased in the simplified glass systems, the coordination of aluminum within the glass structure shifted from 6-coordinated to 4-coordinated (see Figure 1). The implications of this shift are not yet clear, but the change in structure may offer some insight into the mechanisms that reduce the propensity for nepheline crystallization as the concentration of B_2O_3 is increased.

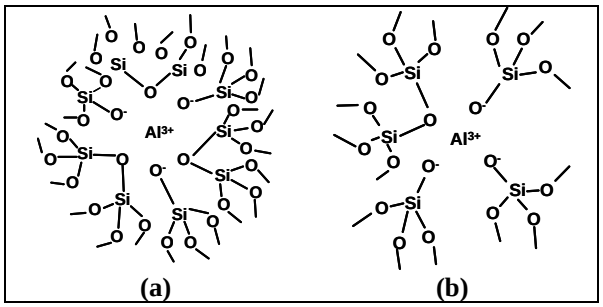

Figure 1. Spectroscopy data indicated a shift from 6-coordinated Al ions (a) to 4-coordinated Al ions (b) as boron concentration was increased in the glass compositions.

Crystallization within the glasses was characterized via X-ray diffraction (XRD). Increased concentrations of B_2O_3 continued to reduce the tendency for nepheline crystallization, while additions of CaO alone (no B_2O_3) did not reduce the amount of nepheline that crystallized. It may be necessary to include both B_2O_3 and CaO in order for CaO to have an effect. It was noted that nepheline tends to crystallize along the surfaces of a glass melt that are in contact with the crucible or furnace atmosphere, while the bulk of the glass may remain amorphous (see Figure 2). It is therefore critical to make sure that sampling of a glass specimen is done in a representative manner when preparing for XRD analysis.

Figure 2. Slowly cooled glass sample showing an amorphous region surrounded by areas of nepheline crystallization.

Varying cooling rates were used to identify crystallization paths in glasses that are known to be prone to nepheline formation. Slower cooling rates allowed for the crystallization of trevorite in an example glass, while faster cooling rates produced an amorphous sample (see Figure 3). Future work will utilize high temperature XRD to monitor changes in crystallization and their subsequent effects on the residual glass composition as samples are cooled.

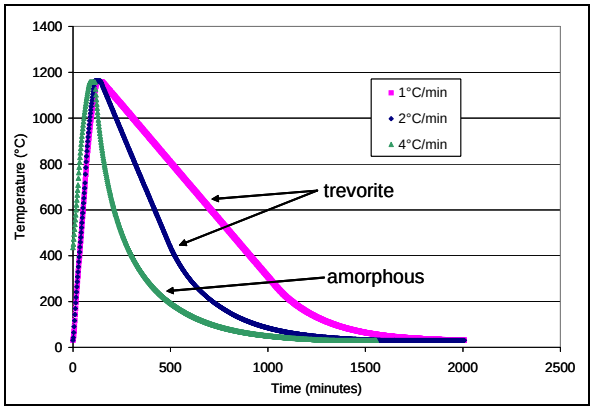

Figure 3. A glass sample cooled at three different rates was amorphous only upon fast cooling.

Zero Interface Catalyst Impregnated Ionomer Membranes for Fuel Cell Applications

D.J. Hathcock, M.C. Kane, and T.M. Adams

- *This program is focused on developing engineered ionomer membrane structures containing embedded nanoparticle catalysts. Increasing the intimate contact between the catalyst and polymer should decrease the transfer barrier associated with typical membrane electrode assemblies.*

Polymer electrolyte fuel cell systems will require significant advances in both performance and cost in order to be competitive with traditional technologies. Current generation polymer electrolyte membrane (PEM) fuel cells suffer from a variety of material limitations including cost, operational efficiency at low humidity, and difficulties in manufacturing complex geometries. Significant research is in progress to develop alternative catalysts to the precious metals presently in use, catalyst-on-membrane technologies, and improved cathode catalysts. Development of efficient, low-cost membranes which can be easily produced in any desired geometry would be a major step towards the commercial realization of on-board fuel cells for hydrogen-powered vehicles.

Most current generation polymer electrolyte membrane (PEM) fuel cells use DuPont Nafion® , a sulfonated derivative of Teflon®, as the proton exchange membrane. While it is the current standard, Nafion® suffers from a number of shortcomings including; limited low relative humidity performance, limited mechanical stability, difficult processing, and high cost. Current PEM fuel cell systems also use significantly more precious metal catalyst than is economical for wide scale deployment. Much effort has been focused on more effective precious metal loading and the development of non-precious metal catalyst systems. Normally the catalyst is applied using traditional methods such as hot pressing, inking, or incorporation onto the gas diffusion layer.

In order for fuel cells to become a commercial reality, it is critical to improve the catalyst activity and lower the precious metal loading. The Department of Energy targets for reformate/air operation are 0.4 A/cm^2 at 0.8V, and 0.1 A/cm^2 at 0.85V. To achieve the MEA cost target of $10/kW for transportation applications, the technology must have the potential to achieve precious metal loadings of 0.2 g/peak kW or 0.05 mg/cm^2. The catalyst used in state-of-art fuel cells is Pt supported on carbon. Current approaches aimed at lowering the Pt loading focus on concentrating Pt where the electrocatalytic reaction takes place. This has been achieved through sputtering and coating the catalyst directly on the membrane. The typical problem with non-precious metal catalysts as a surface layer on the PEM is the mass transport limitations due to the increased thickness of the catalyst layer. The addition of the catalysts into the liquid Nafion® would increase the intimate contact by incorporating the catalyst in the material before cross-linking. By casting a catalyst layer, and casting the next membrane layer on top of it before complete curing/cross-linking of the first layer, the interface can be eliminated and the catalyst incorporated into the proton exchange membrane directly. This method allows separate anode and cathode catalysts to be tailored on each side of the membrane.

In FY08, SRNL conducted experimental work to develop and characterize ionomer membranes containing a nanoparticulate catalyst. Synthesis and production methods using spin coating techniques were developed and the resulting films were characterized using scanning electron microscopy (SEM). Results from SEM imaging (Figure 1 below) show a thin film layer produced, with some attendant domaining visible, via this process. Individual particles within the membranes were not visible due to excessive charging of the polymer.

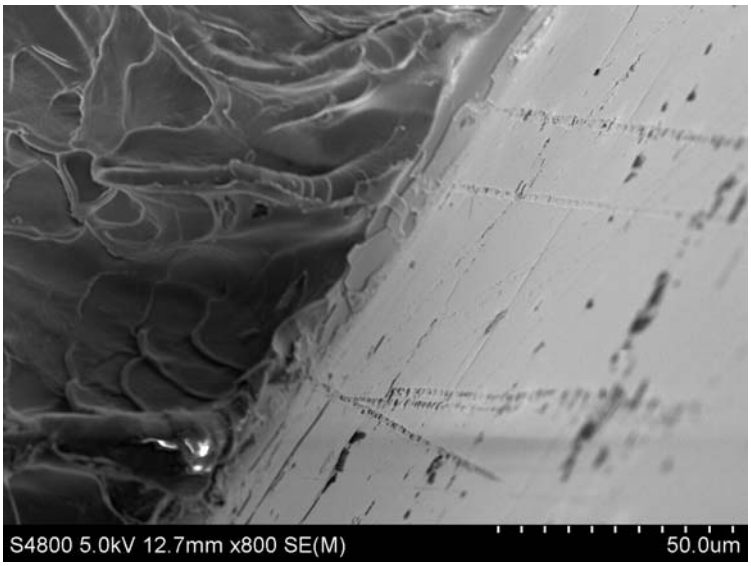

Figure 1- Engineered membrane on Lexan substrate.

Project Summaries Quick Hits

Acceleration of Ion Exchange Kinetics

C. A. Nash

Objective: The goal of this research was to demonstrate kinetics or capacity improvements that alternating voltage might have on ion exchange column breakthrough profiles. Such an effect would be valuable for increasing ion exchange throughput in existing columns. This work placed electrodes in a bed of ion exchange resin so that voltage could be applied and changes in kinetics would be measured. Relative kinetic resistance and capacity factors for each test were calculated by fitting breakthrough data to a standard ion exchange model. Different resin chemistries and electrical voltage/frequencies were used as needed to determine the extent of effect.

Aqueous solutions respond to electric fields with ionic motion. Inducement of ion migration by application of electric fields in the volt per centimeter range is widely known and used in processes like electrolysis, electrophoresis, and water purification with ion-selective membranes. It is expected that accelerated kinetics will be revealed by a sharpening of the breakthrough curve at fixed feed flow rate. Such an effect provides an increase in processing rate for a given feed liquid.

Past work cited in the proposal found that electric fields of 0.05 to 100 kHz enhanced mass transfer in ion exchange membranes. The data suggested that intra-membrane mass transfer resistance was reduced. Resulting resistivity of a deionized water product was more than five times higher than that where little to no field was applied. In separate work electric fields of 0.2 Hz or slower to exchanger membranes to improve water purification. In yet other work low power electric fields (direct current) eluted and regenerated ion exchange particles in a basket after they were used to deionize water.

The experimental work here studied Dowex 21K strong anion resin exchanging hydroxide for chloride, and in addition used resorcinol-formaldehyde (RF) weak acid resin where hydrogen and sodium ions were exchanged. Both resin beds were fed at high flow rates to increase the relative effect of intraparticle mass transfer resistance. Figure 1 shows the electrodes and spacer that was buried in resin when a column was operated.

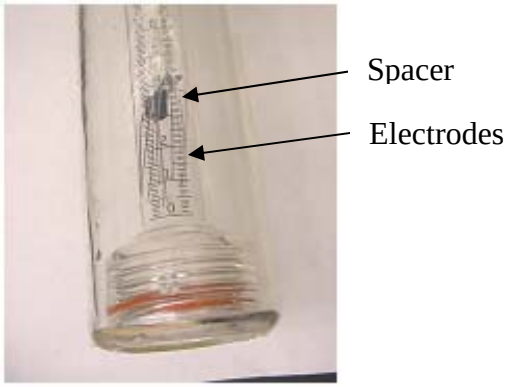

Figure 1. Electrodes and Spacer in an Ion Exchange Column

Control tests never had electricity applied. Three control tests with Dowex 21K provided an average dimensionless capacity of 6.06 +/- 1.6 versus a capacity of 5.94 +/- 2.6 for three electrified bed tests. There was thus no significant change in resin bed capacity. A measure of relative kinetics from a model for the control tests was 0.034 +/- 0.001 versus 0.027 +/- 0.01 for electrified tests.

Results for RF resin are shown in Figure 2. The results may indicate that the relatively high

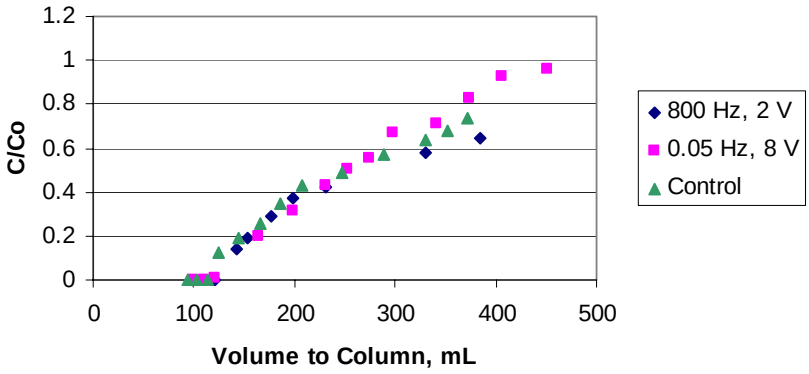

Figure 2. Breakthrough Curves for RF Tests Seeing an Electrical Field (0.1 F nitric acid feed)voltage and/or low frequency (0.05 Hz, 8 V) produced visible improvement, though an experimental technique applied to these tests casts doubt on that conclusion. In tests with electrified beds of RF resin the electricity was

turned on not at the beginning of the test but only at the time when column effluent was dropping below pH 7. This is at the point where a nonzero C/C_0 would first be seen in Figure 2. This was done to see if the commencement of any electrical effect might change the pH coming out of the column. Such an effect was expected around pH 7 when pH is most highly sensitive to chemical changes – hydrogen ion is only 1.E-07 M. In the case of the 800 Hz, 2 V test the voltage was applied when 145 mL of feed had been pumped to the column. In the 0.05 Hz, 8 V test the electricity was turned on when 103 mL of feed had been pumped. Figure 2 shows the data from those two tests along with the control, and no "bump" in the breakthrough curves is evident.

Overall the work finds little evidence of increased resin capacity or kinetics when a bed of resin particles is subjected to alternating voltage. It is likely that the applied current travels through the liquid around the resin particles to an extent that reduces the kinetics improvement. Further work would thus use either ion exchanger membranes or other configurations that reduce the amount of current bypassing the ion exchanger particles.

Enhanced Stabilization and Packaging of Challenging Materials

R.R. Livingston and J.M. Duffey

- This project tests the impact of uranium oxides on headspace gas composition and container pressure during storage of nuclear materials. The addition of uranium oxides to nuclear materials is postulated to mitigate hydrogen gas generation associated with radiolytic decomposition of moisture and may provide an effective alternative to the rigorous stabilization and packaging criteria for nuclear materials.

Safe transportation and storage of challenging materials requires packaging in sealed, robust containers. The limiting condition for packaging many radioactive materials is the potential formation of a flammable hydrogen atmosphere when moisture associated with the content is decomposed by radiation. The safety analysis for transportation and storage of these materials is complicated by the difficulties associated with effectively modeling gas generation and total pressure. Improved understanding of the chemical and radiolytic reactions limiting pressure and hydrogen gas generation is essential to improving gas generation models.

Gas generation experiments are often required to evaluate the headspace gas composition and possible pressure associated with storage of radioactive materials. These experiments are generally limited to measuring the initial gas generation rates prior to reaching equilibrium conditions where the forward rate is balanced by a reverse reaction. These reverse reactions are responsible for limiting the gas composition and pressure that are observed during surveillance of nuclear materials in storage. Improved understanding of these reverse reactions is needed to develop alternative methods for stabilization and storage of challenging materials.

The experiments performed are designed to probe the significant differences in gas generation test observations for plutonium oxide and uranium oxide contents. The large divergence in gas generation behavior from actinide oxides provides the ideal starting point for examining the chemical and radiochemical reactions that limit the hydrogen generation associated with storage of nuclear materials.

The fiscal year 2008 experiments used existing infrastructure and test apparatus for experiments that measure both the gas generation and corrosion of stainless steel materials. Figure 1 provides a cut away view of the test apparatus used in these experiments. The apparatus is fabricated from stainless steel and includes both a transducer for measuring system pressure and valve for sampling or adjusting the headspace gas composition. The temperature and pressure of each vessel are recorded in real-time using a computerized data acquisition system.

Each vessel was loaded in a helium atmosphere with approximately fifty grams of the selected nuclear material. Test materials included uranium oxides (UO_3, U_3O_8), plutonium oxide (PuO_2), and mixtures of these oxides. Samples of each oxide were characterized using x-ray diffraction (XRD) and thermogravimetric analysis (TGA) prior to loading in order to determine chemical composition and moisture content.

Figure 1 - Gas Generation Test Apparatus

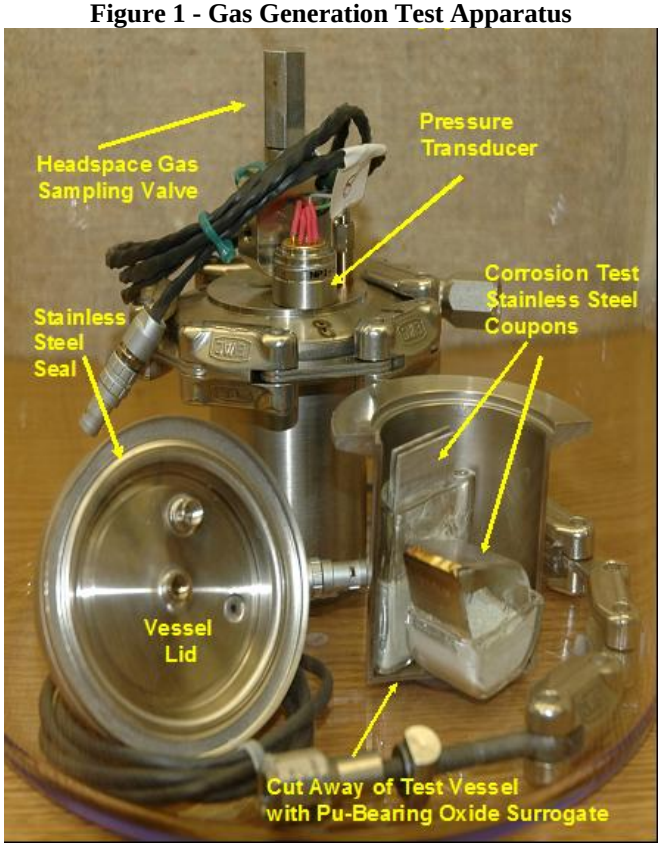

Experiments were initiated by adding approximately 2500 torr helium to each vessel to demonstrate the system was leak tight. Next, the helium was removed and replaced with hydrogen to test the hypothesis that uranium oxides are capable of limiting hydrogen generation associated with radiolysis of moisture. All experiments were conducted at ambient temperature with minimal headspace volume. The pressure of each container was monitored for several weeks to evaluate the effects of oxide composition on hydrogen content.

In each experiment, the uranium oxides showed limited or no ability to remove hydrogen from the test system even at elevated hydrogen pressure. The experimental results for a mixture of uranium and plutonium oxides suggest hydrogen generation was faster than expected based on previous test

results for plutonium oxide with similar moisture content. Consequently, the impact of uranium oxides on hydrogen generation remains ambiguous, and additional experiments are needed to understand how impurities effect the transportation and storage of challenging materials.

Improving Operational Forecasts by Incorporation of Non-Standard Weather Data

S. R. Chiswell and R. L. Buckley

Objective: The goal of this project is to incorporate real-time Doppler radar observations into atmospheric numerical models to improve prognostic forecasting capabilities with specific initial *proof of concept* application to daily Savannah River Site operations and emergency response.

Assimilation of radar velocity and precipitation fields into high-resolution model simulations can improve precipitation forecasts with decreased "spin-up" time and improve short-term simulation of boundary layer winds which is critical to improving plume transport forecasts. During the current year, the United States National Weather Service (NWS) radars will complete a significant upgrade to increase their resolution to 8 times their previous "legacy" resolution, from 1 km range gate and 1.0 degree azimuthal resolution to "super resolution" 250 m range gate and 0.5 degree azimuthal resolution. These radar observations provide reflectivity, velocity and returned power spectra measurements at a range of up to 300 km at a frequency of 4-5 minutes which yield up to 13.5 million point observations per level in super-resolution mode. The migration of National Weather Service (NWS) WSR-88D radars to *super resolution* is expected to improve warning lead times by detecting small scale features sooner with increased reliability; however, current operational mesoscale model domains utilize grid spacing several times larger than the *legacy* data resolution, and therefore the added resolution of radar data can not be fully exploited. The assimilation of *super resolution* reflectivity and velocity data into high resolution numerical weather model forecasts where grid spacing is comparable to the radar data resolution is investigated here to determine the impact of the improved data resolution on model predictions.

Development of software to process NWS radar Level II reflectivity and radial velocity data was undertaken for assimilation of real-time or archived observations into numerical models. In order to prepare the radar observations, a coordinate transformation is performed to convert the radial coordinate data into a volumetric cube. Values are extracted at each point within the cube where data undergo quality control (QC) analysis to eliminate empty / missing data points, decrease anomalous propagation values, and determine error thresholds by utilizing the calculated variances among data values. The Weather Research and Forecasting model (WRF) three dimensional variational data assimilation package (WRF-3DVAR) was used to incorporate the super-resolution data into the WRF input and boundary conditions by formatting the processed radar profiles into vertical point observations.

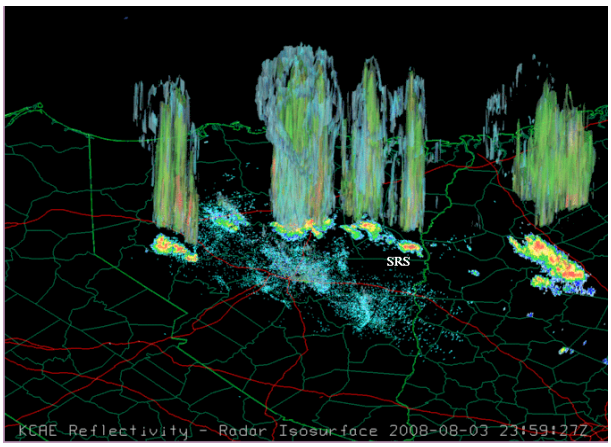

Figure 1. Volume rendering of Level II radar reflectivity from Columbia, SC August 4, 2008 00 UTC viewed from the northwest.

A case study was performed to assess the impact and utility of assimilating super-resolution radar observations, and to develop a methodology for applying the technique for operational use. The Columbia, South Carolina radar location (KCAE) is the closest WSR-88D site in proximity to the Savannah River Site (SRS) and is approximately 91 km (56 mi) NNE of the center of the site. The KCAE radar was upgraded to *super resolution* on July 23, 2008. On August 3, 2008, shortly after KCAE radar began transmitting *super resolution* observations, a weather event typical of mid-summer late afternoon thundershower activity which frequently affects SRS occurred (Fig 1). The time period beginning 00 UTC (Universal Time Coordinated) August 4, 2008 was chosen for a case study since it presented

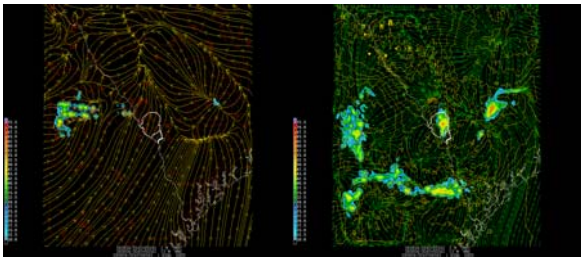

Figure 2. Model simulation of radar reflectivity (shaded areas) and wind streamlines August 4, 2008 00:45 UTC showing base run (Left) and radar assimilation run (Right).

precipitation conditions in and around SRS at the time of the National Center for Environmental Prediction (NCEP) operational model initialization and could highlight the benefit of radar data assimilation. NCEP's operational 12 km resolution North American Mesoscale (NAM) model was used to provide the initial and boundary conditions for local higher resolution model runs centered on SRS. A base run utilizing WRF with a 2.5 km grid and a 0.5 km interior nest grid provided the control for comparison with a second run utilizing radar data assimilation from KCAE at the time of model initialization. Analysis of the model output shows faster spin up to precipitation when radar data is assimilated. By 45 minutes into the model runs, there is little convection in base case, while there is considerable established convection in the radar initialized run. Model output from the radar run shows an established thunderstorm cell over eastern and southeastern SRS (Fig 2).

In order to compare model simulated winds with 15 minute observed wind measurements recorded from SRS meteorological towers, a site average for both 10m above ground level and the lower boundary layer was computed from the instantaneous wind fields generated at each output time of the model runs. Comparison of these fields reveal that the radar assimilation run provides a better agreement during the first 6 hours of simulation, after which, both the assimilation and base runs show little difference due

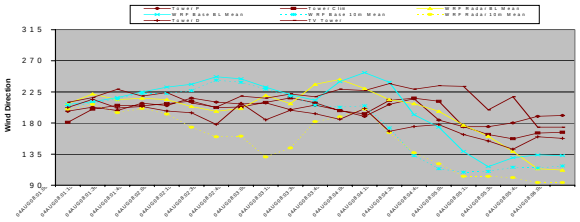

Figure 3. Wind direction from SRS observations (brown), base run (blue) and radar initialized run (yellow) for 0100-0600 UTC August 4, 2008.

to the dissipation of convective activity and a return to weakly driven nighttime flow (Fig 3).

The Hybrid Single-Particle Lagrangian Integrated Trajectory (HYSPLIT) model was used to generate transport of a hypothetical atmospheric contaminant release using forecast winds for the two model simulations. Surface concentration was calculated assuming effluent within the lowest 50 meters above ground. Turbulence was calculated using the horizontal and vertical velocity variances within the mesoscale model, while removal processes were not considered. The general pattern of both runs is indicative of the larger scale southwesterly transport direction with initial meandering due to the outflow of storms located to the south and west. The primary affect of the generation of convection in the vicinity of SRS prior to 02 UTC in the assimilation case is increased plume spread and slightly lower maximum surface concentrations. The arrival of the cold air pool driven by thunderstorm outflow is seen in both runs between 3Z and 8Z as an abrupt shift to winds from the east. By comparison, the radar assimilation case shows a large area of fumigation which spreads over two-thirds of the SRS site area while the base case shows considerably less areal spread. The period of rapid fumigation occurs coincident with the period where the 10 m and lower boundary layer model wind directions show the greatest differences.

Conclusions:

The spin-up time for precipitation was observed to be less when radar data was assimilated. The lack of observational data in the vicinity of SRS available to NCEP's operational models signifies an important data void where radar observations can provide significant input. These observations greatly enhance the knowledge of storm structures and the environmental conditions which influence their development. As the increase in computational power and availability has made higher resolution real-time model simulations possible, the need to obtain observations to both initialize numerical models and verify their output has become increasingly important. The assimilation of super resolution radar observations therefore provides a vital component in the development and utility of these models.

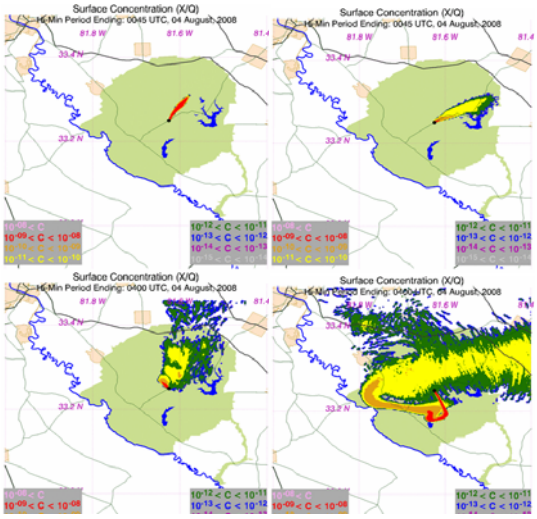

Figure 4. HYSPLIT runs for base case (left) and radar assimilation case (right) depicting concentrations at 45 minutes (top) and 4 hours (bottom) for a simulated release within SRS.

Structural and Electrical Characterization of Organic Materials in Organic-Based Devices

Principal Investigator: *Lucile C. Teague, Savannah River National Laboratory, Aiken, SC 29808*
Other Investigators and Collaborators: *Oana D. Jurchescu[1,2], Curt A. Richter[1], David J. Gundlach[1], James G. Kushmerick[1], Sankar Subramanian[3], John E. Anthony[3], Thomas N. Jackson[2], Xinran Zhang[1] and Dean Delongchamp[1]*

[1]NIST, Gaithersburg, Maryland, [2]The Pennsylvania State University, State College, PA, [3] University of Kentucky, Lexington, KY

Objective: Scanning Kelvin probe microscopy (SKPM) was utilized to study charge transport in organic-based devices, correlating the electrical response with the structure of the organic material. This work is motivated by the demand for high-performance, low power, and low-cost device structures that can be utilized for a wide range of applications. There is significant interest in comparing the structural and electronic properties of devices made from different manufacturing and deposition/processing methods and from different organic materials. Our studies focused on organic-based devices made from both single crystal (SC) organic materials[1] and ink-jet printed organic materials in order to gain a better understanding of the relationship between the electrical performance and structure of organic thin-film transistors (OTFTs).

SKPM Studies on Single Crystal Organic Field Effect Transistors: SC-OTFTs made from two different acene derivatives were studied using SKPM, correlating the electrical response with structure of the organic material down to the microscale. Briefly, SKPM was used to obtain a spatially resolved surface potential map of operating organic devices that employed diF-TES-ADT[a] or diF-TIPS-ADT[b] SCs as the active organic semiconductor. SKPM imaging at the electrode/organic interface allowed for the investigation of charge injection at the source and drain contacts. Drain-source voltages (V_{DS}) and gate voltages (V_G) were applied to devices (mounted in a ceramic DIP) with a semiconductor parameter analyzer. The transistor transport and transfer characteristics were also measured for each device immediately before and after SKPM scanning.

Figure 1 shows the transport characteristics and SKPM data for a diF-TES-ADT SC-OTFT (~ 150nm thick crystal). The SKPM image indicates ~1.5V drop in potential at the contact edge (V_{DS} = -10V, V_G = -40V) which indicates a small barrier to charge injection in the device. These results are consistent with the measured transport characteristics. Using the SKPM data, these contact effects can be accounted for and the true charge mobility in the device can be calculated. For this device, the calculated charge mobility is ~ 2 $cm^2/V*s$.

SC-OTFTs made from diF-TIPS-ADT were also investigated. In contrast to the diF-TES-ADT devices, diF-TIPS-ADT devices show a dramatic increase in the contact effects over time. SKPM imaging of these devices show that 80-90% of the voltage drop in the device occurs at the source contact. At present, what causes these large differences in device stability, and ultimately the device performance for the two different materials is unclear.

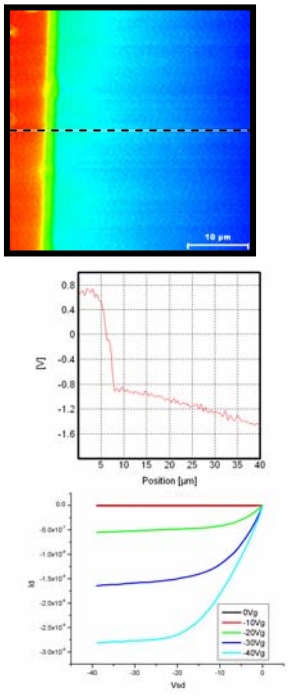

Figure 1. SKPM and transport characteristics (bottom) for an operating diF-TES-ADT SC-OTFT (V_{DS}=-10V, V_G=-40V). Dotted line in SKPM image (top) indicates area of line profile shown (center). For this device, a small potential drop is observed at the contact edge indicating a barrier to charge injection at the contact.

Preliminary Studies on Ink-jet Printed Devices: Using a commercially available research-grade ink-jet printer, diF-TES-ADT patterns were printed onto a variety of substrates and subsequently imaged using optical microscopy and AFM. 10pL droplets of 1 wt% diF-TES-ADT in toluene generated by the print head were used to print a test pattern of lines of increasing width onto a flexible overhead transparency, a clean SiO_2 surface (100nm thermal oxide), an OTS treated SiO_2 substrate, a clean Au

surface and an Au surface treated with pentaflurobenzene thiol.

Optical imaging of these printed surfaces revealed that diF-TESADT could be printed on all surfaces, with the exception of the OTS treated SiO_2. The images in Figure 2 show optical images of some of the different printed line structures, the thinnest of which is ~100µm (1 droplet wide). While some crystalline regions of printed material are observed, there is a lack of continuity along the vertical length of the line. For wider lines, crystalline regions are observed along the horizontal length of the line where several droplets are printed in a row. The observed difference in continuity of the printed material (vertical vs. horizontal) is most likely due to the method in which the pattern is printed on the substrate and elapsed time for solvent evaporation between printed droplets.

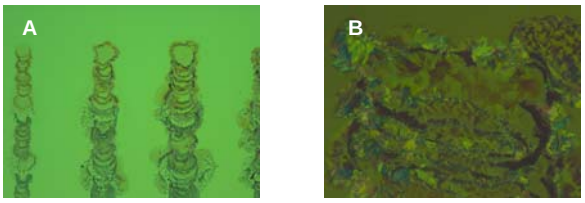

Figure 2. Optical micrographs of diF-TESADT printed on treated Au substrate. (A) 5X magnification image of lines of varying width. Leftmost line is 1 droplet wide. (B) 20X magnification of line showing some crystalline regions formed.

Following these initial tests, shorter lines of diF-TESADT, one droplet wide, were printed on a SiO_2 thermal oxide substrate patterned with Au source and drain contacts at a variety of substrate temperatures. The uniformity and crystalline structure of the printed line were found to increase with increasing substrate temperature, most likely due more rapid evaporation of the solvent. These printed devices were examined by optical microscopy and their transistor characteristics were also probed (Figure 3). Electrical measurements reveal that all of the printed devices show transistor-like behavior, however, they have very low charge mobilities (~10^{-2} $cm^2/V*s$).

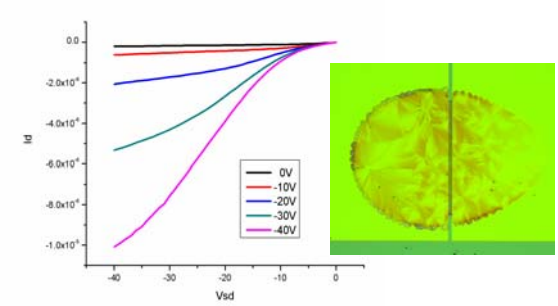

Figure 3. Transport characteristics and optical image of an ink-jet printed transistor) printed at 40ºC substrate temperature. Channel length is 20 µm. Optical images reveal crystalline structure and the measured transport characteristics show contact effects.

Conclusions: The work described herein focused on SKPM measurements of electrically active, single-crystal organic-based devices from two similar acene derivatives. Studies of the structural and electronic properties of diF-TES-ADT SC devices provide a comparison to previous SKPM studies of spun-cast thin film transistors.[2, 3] These results will be prepared for submission to a peer-reviewed journal.

This work also provided preliminary data on ink-jet printing of these materials toward the development of new low-cost large-area electronics. Ink-jet printing of organics has the promise to be used for devices on more flexible substrates such as fabrics and plastics. More work in this area is needed to test a variety of deposition/printing conditions as well as substrate materials (i.e., flexible substrates).

Description of Research Partnership: SC and ink-jet printed organic-based devices for this study were prepared and tested at NIST. SRNL researchers used SKPM to analyze the structural and electrical properties of these devices. The active organic materials used to create these devices were synthesized at the University of Kentucky.

References:

1. Jurchescu, O. D.; Subramanian, S.; Kline, R. J.; Hudson, S. D.; Anthony, J. E.; Jackson, T. N.; Gundlach, D. J., Organic single crystals field-effect transistors of a soluble anthradithiophene. **submitted**.

2. Gundlach, D. J.; Royer, J. E.; Park, S. K.; Subramanian, S.; Jurchescu, O. D.; Hamadani, B.; Moad, A. J.; Kline, R. J.; Teague, L. C.; Krilliov, O.; Richter, C. A.; Kushmerick, J. G.; Richter, L. J.; Parkin, S. R.; Jackson, T. N.; Anthony, J. E., contact induced crystallinity. *Nature Materials* **2008,** 7, (216-221).

3. Teague, L. C.; Hamadani, B.; Jurchescu, O. D.; Subramanian, S.; Anthony, J. E.; Jackson, T. N.; Richter, C. A.; Gundlach, D. J.; Kushmerick, J. G., *Adv. Mater*. **in press**.

[a] Triethylsilylethynyl- anthradithiophene
[b] Triisoprophylsilylethynyl-anthradithiophene

The Effect of Magnetic Field and Magnetic Field Type on the Uranium and Strontium Sorption on Monosodium Titanate

F. F. Fondeur, D. T. Hobbs, and S. D. Fink

Objective: This research explored the feasibility of using permanent magnetic fields to enhance the sorption rate of uranium and strontium on monosodium titanate (MST). The results indicate a 25% to 100% enhanced sorption rate of uranium and strontium on MST under the presence of a gradient magnetic field (397 Gauss/m). No effect was detected under a homogeneous magnetic field.

The Savannah River Site (SRS) is currently using MST for removing actinide and strontium from radioactive aqueous waste. The sorption takes approximately three months to reach equilibrium conditions. To compensate for the slow sorption kinetics, personnel mix the slurry and use fresh MST batches after 24 hours of contact time. This strategy increases energy costs and increases the waste generated from the large inventory of the partially loaded MST particles. The slow kinetics results in larger equipment than desired and limits processing throughput. A low cost method is needed to speed actinide and strontium sorption on MST.

Recent research shows that magnetic fields can disrupt the hydrogen bonding of water. The water inside pore spaces form a hydrogen bonded network that retards ion transport. Breaking the hydrogen bonding network may facilitate actinide and strontium adsorption. MST is known to contain porous network of fibrous material. The goal of this work was to determine the effect of different magnetic fields such as a gradient magnetic field and a spatially homogeneous magnetic field on actinide and strontium sorption on MST.

Personnel purchased two permanent magnets (Fe-Nd-B) of the same magnetic field strength (0.9 Tesla) but in one magnet the field decays linearly with distance at 397 Gauss per meter (monopole) while in the other magnet the field is homogeneous throughout the gap between the poles (dipole). A simulated salt solution containing depleted uranium, strontium (^{88}Sr), and 0.8 g/L MST was placed (a known distance) next to the dipole or at the mid-point gap of the dipole and then spun at 30 and 300 rpm (i.e., Reynolds number of 222 and 2.2 E3, respectively).

Figure 1 shows the uranium loading on MST after 2 hours of contact with MST ([MST] = 0.8 g/L). Inspection of Fig. 1 clearly shows that a gradient magnetic field enhanced the sorption of uranium on MST. process to load the resins more and process more aqueous solutions.

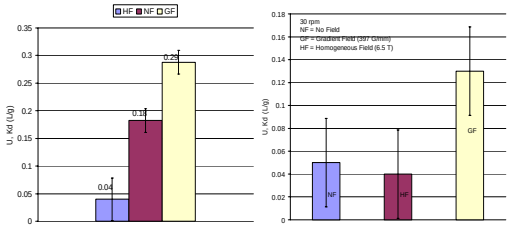

Figure 1. The effect of the magnetic field type on the rate of sorption of uranium on MST after 2 hours of contact with MST. A gradient field sped up uranium sorption. Key: NF = No Field, HF = Homogeneous Field, and GF = Gradient Field.

A similar conclusion is observed for strontium that sorbed faster on MST under a gradient magnetic field as shown in Figure 2.

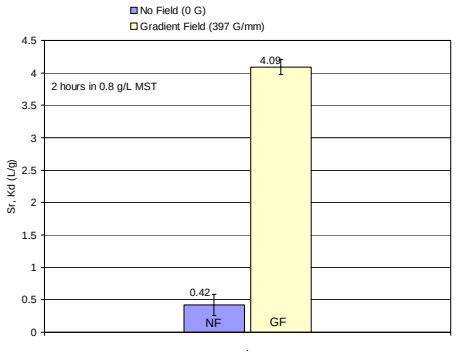

Figure 2. The effect of a gradient magnetic field on the rate of strontium loading on MST (spun at 30 rpm).

The enhanced sorption rate of uranium and strontium on MST in the presence of a magnetic field gradient can be due to additional solution mixing action outside the MST particles originating from additional forces (i.e., Lorentz and diamagnetic forces) due to the electrical conductivity of the salt solution and the

diamagnetic property of water. However, recently published work shows that these forces retard natural convection (driven by temperature gradients) in enclosures. In other words, the enhanced sorption seen in this work can not be explained with enhanced mixing outside of the MST particles.

We believe the enhanced sorption rate is occurring within the pore space of MST. The solution chemistry inside the pores (such as ionic strength) may be different from the solution chemistry outside the MST particles due to size exclusion of hydrated ions and release of hydroxide and sodium ions in the region of the ion exchange sites. This gives the pore solution chemistry a different magnetic and electrical property from the bulk solution. Therefore, under a magnetic field gradient, the solution in the pores may experience additional forces that can break the hydrogen bonding of water and lead to convective flow (thus lowering the diffusion resistance within the pores).

The implication of this finding indicates that the ion exchange process in packed bed column can be enhanced by placing a permanent magnet in the packed column in such a way that the field is opposite to the direction of the solution flow in the packed bed. The authors also envision placing an electromagnet winding around an ion exchange resin column in such a way as to create an alternating magnetic (on and off) for the solution flowing past the ion exchange bed and shorten the mass transfer zone of the ion exchange.